CHAPTER D-8 SEISMIC RISKS FOR EMBANKMENTS

D-8.1 Key Concepts

There have been very few instances where an earthquake has damaged an embankment dam enough to result in the uncontrolled release of reservoir water. Many embankment dams are exposed to earthquake shaking each year, but either the damage caused by the earthquake has not been extensive enough, or in the rare cases where damage was extensive, many of the reservoirs were, by chance, low at the time of the earthquake, so uncontrolled releases did not happen. The failure probability estimation procedures described below are built upon standard analysis techniques used to predict responses of soil to dynamic loading and upon observations from case histories of embankments that have been exposed to earthquakes.

Dynamic loading can cause permanent deformation if the stress changes cause shear or tensile strength to be exceeded. Loose, saturated, cohesionless soils, when subject to earthquake shaking and initial shearing, can contract as the soil particles are rearranged. Since the water within the pore spaces is virtually incompressible, this results in an increase in pore water pressure and decrease in shearing resistance. If the pore pressure increase is enough to reduce the effective stress to nearly zero, the soil is said to have liquefied, and the soil experiences a significant reduction in shear strength. Extensive shear strength reduction beneath an embankment slope can trigger a flow slide which, in turn, can result in a very rapid dam failure. In dense, saturated cohesionless soils, large shear displacements may not occur. Instead, the temporary occurrence of excess pore water ratios of 100 percent (or initial liquefaction) is accompanied by the development of limited strains, resulting in progressive and incremental lateral spreading of slopes.

Whether or not the soil of an embankment or its foundation liquefies completely, pore pressure can increase, resulting in a decrease in shearing resistance. If enough reduction occurs, over a sufficient extent, large deformations can result. Translational failure can occur if the entire foundation beneath an embankment liquefies and the reservoir pushes the embankment

downstream far enough to create a gap it can flow through. Overtopping erosion failure can occur if crest deformations exceed the freeboard at the time of the deformations.

If the deformations do not result in an immediate release of the reservoir, the embankment can be cracked or disrupted to the point where internal erosion can occur through the damaged remnant. This failure mechanism can occur with or without liquefaction. There are many ways in which cracking can occur due to seismic shaking, such as differential settlement upon shaking, general disruption of the embankment crest, offset of a foundation fault, or separation at spillway walls. See Chapter IV-4 Internal Erosion Risks for Embankments and Foundations for other conditions that may make a particular dam more susceptible to transverse cracking and subsequent internal erosion.

Compacted embankments are typically not considered susceptible to liquefaction upon shaking and initial shearing. Dense, cohesionless soils tend to dilate upon shearing, which increases the pore space between soil particles and reduces the pore pressures. Most Reclamation and USACE embankment dams are compacted, so the focus of liquefaction studies tends to be related to loose foundation soils.

However, hydraulic fill embankments may be susceptible to liquefaction or pore pressure increases. Fine-grained soils, while not strictly “liquefiable,” may be susceptible to strength loss during an earthquake. Two aspects of a fine-grained soil's shear strength behavior can require investigation: 1) the anticipated peak magnitude of earthquake-induced shear loading when compared to a soil's undrained shear strength determined from monotonic loading; and 2) sensitivity, which is the potential for a reduction in the undrained shear strength due to the effects of many shearing cycles or very large monotonic strain.

If active faults or faults capable of co-seismic displacement cross an embankment dam foundation, the potential exists for foundation displacement that cracks or disrupts the dam core or water retaining element as well as transition zones or filters. The cracking can initiate concentrated seepage, and the translational movement can create locations where there would be unfiltered exit points for the seepage. Both conditions would increase the likelihood for failure from internal erosion. Shearing of a conduit passing through an embankment dam as a result of

fault displacement can result in transmission of high pressure water into the dam, leading to increased gradients and potential for internal erosion. At the time of the 1906 San Francisco Earthquake, Upper and Lower Howell Creek Dams were located on the San Andreas Fault and holding water. Lower Howell Creek Dam which had a conduit through it failed, but Upper Howell Creek with no conduit did not. The presence of the conduit *might* have made the difference.

Seiche waves can be generated by large fault offsets beneath the reservoir, by regional ground tilting that encompasses the entire reservoir, or by mass instability or slope failure along the reservoir rim. “Sloshing” can lead to multiple overtopping waves from these phenomena.

D-8.2 Important Case Histories

Relatively few dams have actually failed as a result of liquefaction, internal erosion through seismically induced cracks, or other seismic failure modes. However, a few case histories provide relevant insights.

D-8.2.1 Lower San Fernando Dam (1971)

The upstream slope of Lower San Fernando Dam failed during the 1971 San Fernando Earthquake (Seed et al. 1975). Intact blocks of embankment material moved tens of feet on liquefied hydraulic fill shell material (Figures D-8-1 and D-8-2). There was evidence to suggest the slope failure took place after the shaking had stopped. Fortunately, a remnant of the dam remained above the reservoir water level at the time, and the dam did not breach.

Figure D-8-1. Lower San Fernando Dam after 1971 Earthquake (Courtesy of National Information Service for Earthquake Engineering, University of California, Berkeley, Karl Steinbrugge Collection)

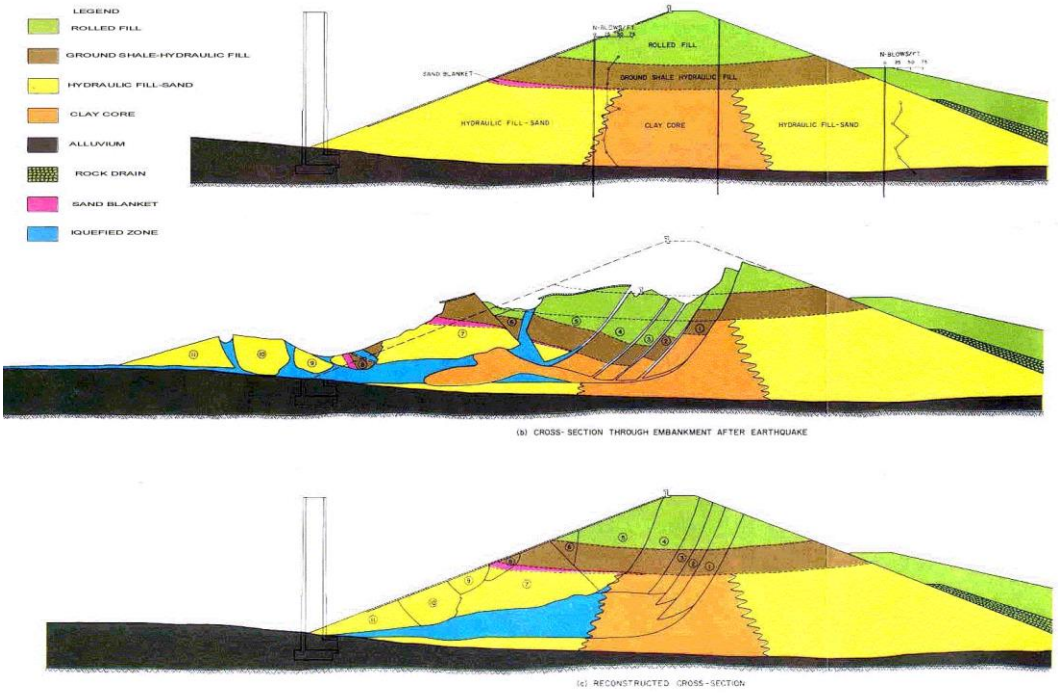

Figure D-8-2. Cross Section of Lower San Fernando Dam before and after Earthquake (Seed et al. 1975)

D-8.2.2 Sheffield Dam: 1925

Sheffield Dam failed during the Santa Barbara earthquake of 1925 (Figure D-8-3). Although there were no witnesses to the breach, it was believed that the sandy foundation soils which extended under the entire dam liquefied and that a 300-foot long section of the dam slid downstream, perhaps as much as 100 feet (Seed et al. 1969). The dam was located quite close to the city of Santa Barbara, and a wall of water rushed through town, carrying trees, automobiles, and houses with it. A muddy, debris-strewn aftermath was left behind. Flood waters up to 2 feet deep were experienced in the lower part of town before they gradually drained away into the sea. No fatalities were reported.

Figure D-8-3. Sheffield Dam after 1925 Earthquake
(Courtesy of National Information Service for Earthquake Engineering, University of California, Berkeley)

D-8.2.3 Cracking of Dams Exposed to Loma Prieta Earthquake (1989)

Harder (1991) describes the damage that occurred to 35 dams exposed to the Loma Prieta Earthquake. The Loma Prieta Earthquake was a magnitude 7.0 earthquake with approximately 7 to 10 seconds of strong shaking. Dams exposed to less than 0.2g did not experience damage.

Dams exposed to peak ground accelerations between 0.2g and 0.35g either experienced no damage or developed longitudinal cracks. Transverse cracking was only noted in dams exposed to greater than 0.35g, although 7 of 19 dams exposed to this level of shaking experienced no damage, 7 of 19 dams experienced either minor or longitudinal cracking, and only 5 of 19 dams experienced transverse cracking. Only Austrian Dam suffered severe damage.

D-8.2.4 Austrian Dam (1989)

Austrian Dam was severely cracked and damaged by the 1989 Loma Prieta Earthquake (Forster and MacDonald 1998), with peak ground accelerations estimated at 0.5g to 0.6g from the nearby magnitude 7 event (Figures D-8-4 and D-8-5). Longitudinal cracks that were 14 feet deep (based on trenching) formed just below the dam crest on the upstream and downstream slopes. Transverse cracks formed at both abutments, 1 to 9 inches wide, and the embankment separated from the concrete spillway wall, opening a gap of about 10 inches. Fortunately, the reservoir was low at the time of the earthquake, and no subsequent internal erosion ensued.

Figure D-8-4. Settlement and Cracking at Austrian Dam in Area of Spillway Wing Wall (Courtesy of Sal Todaro)

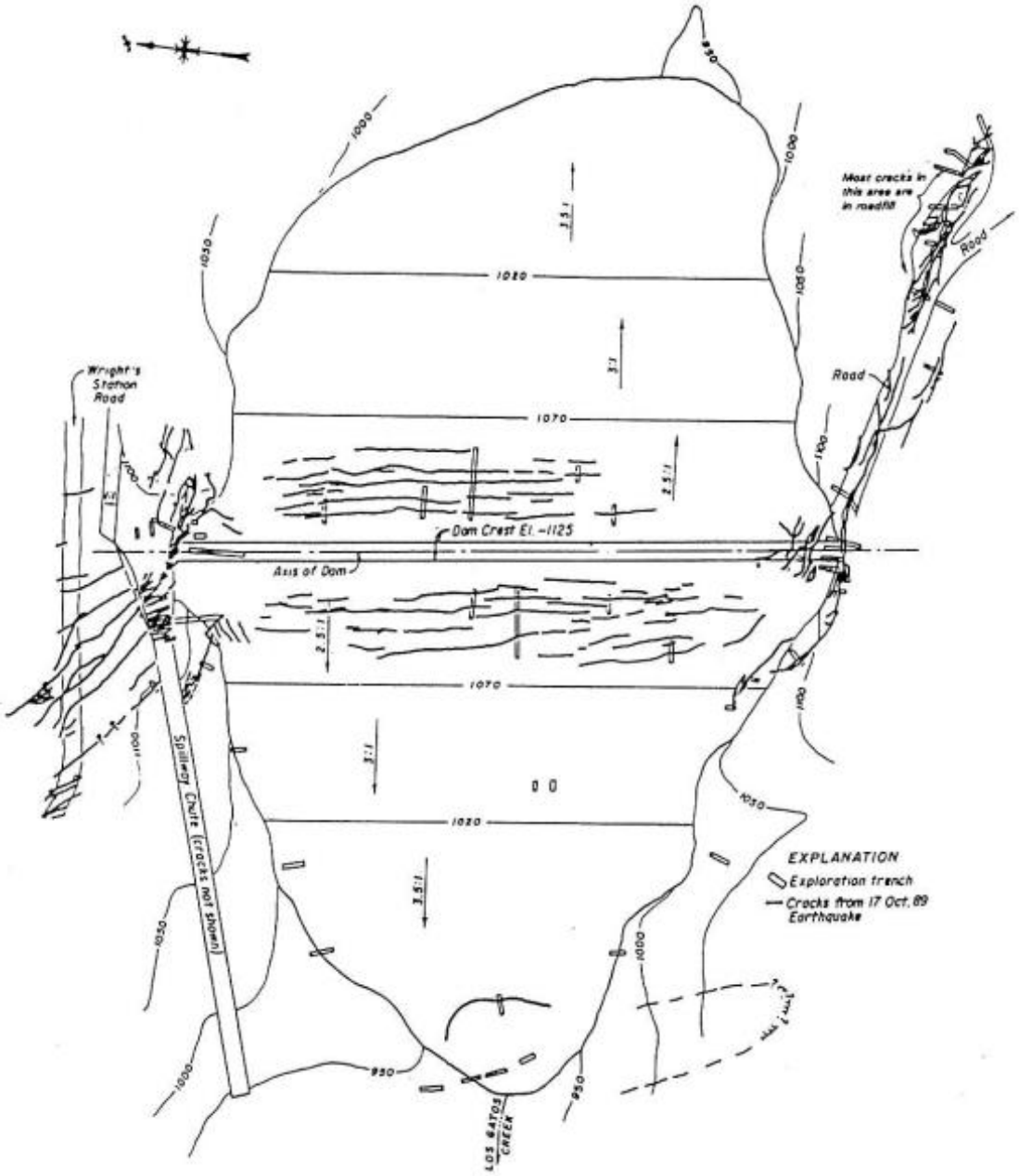

Figure D-8-5. Plan of Transverse and Longitudinal Cracking at Austrian Dam (Forster and MacDonald 1998)

D-8.2.5 San Fernando Power Plant Tailrace Dam (1994)

A small embankment dam forming the tailrace for the San Fernando power plant was shaken by large ground motions during the 1994 Northridge earthquake. The earthquake occurred early in the day, and the tailrace dam was intact when power plant personnel left for the day. The next morning, the dam had failed (Davis 1997). The tailrace concrete lining had buckled in several

locations. It was suspected that a layer of loose sand beneath the dam, identified by CPT data, liquefied, and piped through the gaps in the concrete lining undetected, slowly throughout the day.

D-8.3 Steps for Risk Evaluation

The general steps for evaluation of seismic risks for embankments are as follows:

- Develop detailed site-specific potential failure modes
- Develop event trees to assess the potential failure modes
- Establish loading conditions for earthquake ground motions and associated magnitudes, as well the coincident reservoir level
- Evaluate site conditions and develop representative characterization of the embankment and foundation materials
- Perform a screening by evaluating the load combinations and site characteristics to determine if seismic potential failure modes will be significant risk contributors

If the potential failure mode can't be screened out, then perform the following for each selected earthquake and reservoir load combination.

- Estimate the likelihood of liquefaction of any foundation or embankment materials
- Calculate the likelihood of no liquefaction (one minus the probability of liquefaction)
- Estimate the residual strength of the materials that may liquefy or may experience strength loss
- Estimate the deformation of the embankment given liquefaction
- Estimate the deformation of the embankment given no liquefaction occurs

For overtopping, assess the estimated deformation, and estimate a probability of overtopping. Different estimates are made for the various reservoir (freeboard) and earthquake combinations represented in the event tree. Complete the event tree nodes following procedures similar to flood overtopping failure modes. See Chapter IV-2 Flood Overtopping Failure.

For cracking, assess the estimated deformation, and determine the likelihood of developing transverse cracks. Estimate the depth and width of the cracks, and complete the event tree similar to the failure mode of internal erosion through cracks. See Chapter IV-4 Internal Erosion Risks for Embankments and Foundations.

The probability for each node in the event will be determined by expert elicitation considering all of the more likely and less likely factors associated with that node. See Chapter I-6 Subjective Probability and Expert Elicitation.

D-8.4 Seismic Potential Failure Modes

The following are generic descriptions of how a dam might fail due to these potential failure modes. For a specific dam, additional details would be needed in the descriptions, as described in the Chapter I-3 Potential Failure Mode Analysis.

D-8.4.1 Deformation and Overtopping

Severe earthquake shaking causes loose embankment or foundation materials to contract under cyclic loading, generating excess pore water pressures (i.e., liquefaction occurs). The increase in pore water pressure reduces the soil's shear strength. (This could also occur as a result of loss of strength in a sensitive clay.) Loss of shear strength over an extensive area leads to slope instability and crest settlement. Crest deformation exceeds the freeboard existing at the time of the earthquake. The depth and velocity of water flowing over the crest are sufficient to erode materials covering the downstream slope. Headcutting action carves channels across the crest. The channels widen and deepen. Subsequent human activities are not sufficient to stop the erosion process. The embankment breaches and releases the reservoir.. If the seismic deformation is great enough for the crest to settle below the reservoir level, overtopping can be initiated. This mostly pertains only to dams that have a small amount of freeboard at the time of the earthquake. If the freeboard at the time of the earthquake is small enough, this failure mode could also occur without liquefaction, particularly if there is soft or sensitive clay in the foundation.

D-8.4.2 Deformation and Transverse Cracking at the Crest

Severe earthquake shaking causes loose embankment or foundation materials to contract under cyclic loading, generating excess pore water pressures (i.e., liquefaction occurs). The increase in pore water pressure reduces the soil's shear strength. Loss of shear strength over an extensive area leads to slope instability, deformations, and crest settlement. However, crest deformation does not exceed the freeboard existing at the time of the earthquake. Open and continuous transverse cracks form across the crest and through all zones of the dam deep enough to intersect the reservoir. The depth and velocity of water flowing through the open cracks are sufficient to erode the materials along the sides and across the bottom of the cracks. Material from upstream zones is not effective in sealing the cracks (by being transported to a downstream zone or constriction point where a filter would begin to form). Headcutting action carves channels across the crest. The channels widen and deepen. Subsequent human activities are not sufficient to stop the erosion process. The embankment breaches and releases the reservoir. This failure mode can also be initiated without the requirement for liquefaction. If the seismic deformation is great enough for cracking to extend to the below the reservoir level, internal erosion can be initiated. Again, this mostly pertains only to dams that have a small amount of normal freeboard, such as a water supply dam that is kept full most of the time.

D-8.4.3 Liquefaction and Sliding Opening Gaps

Severe earthquake shaking causes loose embankment or foundation materials to contract under cyclic loading, generating excess pore water pressures (i.e., liquefaction occurs). The increase in pore water pressure reduces the soil's shear strength. (Again, this same outcome could occur if there is sensitive clay in the foundation.) Loss of shear strength occurs in a layer that is continuous upstream to downstream. Reservoir loading exceeds the shearing resistance remaining in the layer, and the entire embankment slides downstream. Downstream deformation opens a gap at the crest deep enough to intersect the reservoir. The depth and velocity of water flowing through the gap are sufficient to erode the materials along the sides and across the bottom of the gap. Material from upstream zones is not effective in sealing the gap (by being transported to a downstream zone or constriction point where a filter would begin to form). Headcutting carves channels across the crest. The channels widen and deepen. Subsequent human activities are not sufficient to stop the erosion process. The embankment breaches and

releases the reservoir. It is believed that Sheffield Dam failed by this mechanism in the 1925 Santa Barbara CA earthquake.

D-8.4.4 Deep Cracking

Severe earthquake shaking causes differential settlement over stiffness discontinuities, at near-vertical embankment-foundation contacts, or at contacts between the embankment and concrete. Continuous transverse cracks of sufficient width form through the core, and concentrate seepage flow through the cracks below the reservoir level occurs. The seepage quantity and velocity are sufficient to erode core material and transport it beyond the downstream shell material. Upstream zones are not effective in sealing the cracks (by a mechanism whereby material from upstream zones would be transported to a downstream zone or constriction point where a filter would begin to form). Subsequent human activities are not sufficient to stop the erosion process. The embankment breaches and releases the reservoir.

D-8.5 Screening

Screening of seismic potential failure modes can be done by evaluating both the probabilities associated with the load combinations, the characteristics of the dam features, and the embankment and foundation materials. Teams should assess the combined probabilities of the seismic and reservoir loads early in the process. Often for flood risk management dams (or dams with flatter slopes and large normal freeboard), the seismic potential failure modes can be screened out just on the basis that the loading required to make the failure mode credible is so remote that it will not drive the project risk. A good knowledge of case histories related to dam performance during earthquakes is essential to help guide the judgment of the team.

There are factors associated with the loading and dam characteristics that make seismic potential failure modes more likely or less likely (adapted from Seed et al. 1975).

More likely factors for damaging deformation:

- PHA greater than 0.2g
- Capable faults beneath the embankment
- Hydraulic fill embankments

- Saturated sand embankments
- Loose, saturated alluvial foundations
- Fine-grained soils susceptible to cyclic failure
- Thin impervious cores
- Thin filter zones
- Conduits embedded in embankment
- History of seismic damage
- Earth embankment-concrete section interface
- Small freeboard

Less likely factors for damaging deformation:

- PHA less than 0.2g
- No capable faults beneath embankment
- Well-built, rolled/compacted embankments (i.e., RC > 95 percent or D_r > 75 percent)
- Non-liquefiable embankment and foundation materials (i.e., embankment founded on rock, dense foundation soils with $(N_1)_{60}$ > 30 bpf, or foundation materials are non-sensitive clays)
- Unsaturated embankment and foundation soils
- Embankment slopes flatter than 3H:1V
- Large core and filter zones
- Rock fill shells
- Static factor of safety against slope instability greater than 1.5
- Freeboard greater than 3 to 5 percent of the embankment height and low seismicity
- No embedded critical features that would be harmed during small embankment movements

D-8.6 Event Tree

Figure D-8-6 shows an example event tree for a single seismic failure mode, overtopping due to liquefaction and large settlement of the crest. At the first node, the tree splits into four branches representing the annual probability of different levels of earthquake loading, in the form of selected ranges of peak horizontal ground acceleration (PGA) or other measure of earthquake

shaking. Each of those branches splits again for different levels of the reservoir that would exist at the time of the earthquake; the probability assigned to each reservoir range is based on historic or expected reservoir operations. (The choice of whether to put the earthquake loading first or the reservoir loading first is simply a matter of which is more convenient in a particular case). Now, aside from the branch for earthquake loading too small to lead to failure (less than 0.1g in the example), there are twelve loading ranges that could lead to failure (i.e., four different reservoir ranges with each of three different PGA ranges). The remainder of the event tree is for estimating the probability of a breach given each of the twelve loadings.

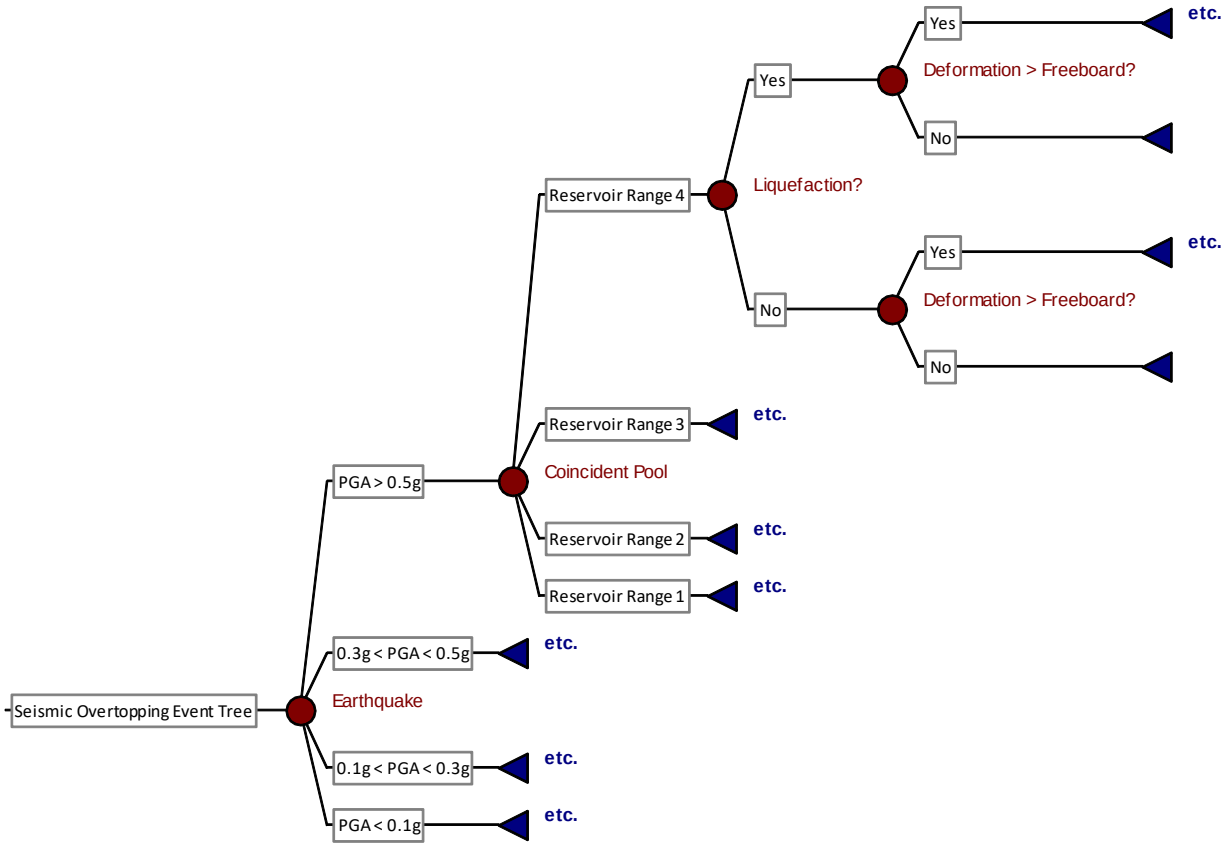

Figure D-8-6. Example Seismic Event Tree

At the node for each of the twelve loading cases, there are branches for widespread liquefaction of foundation soils and no widespread liquefaction. Each of those leads to two possible outcomes: deformation exceeding the available freeboard, making failure of the dam by overtopping flow quite likely, or deformation less than the freeboard, in which case the dam

could fail by internal erosion through cracks, or not fail at all. The probability of failure by internal erosion through cracks can be assessed by essentially the same methods as for internal erosion in normal operation, described in Chapter IV-4 Internal Erosion Risks for Embankments and Foundations, modified for seismic loading. (That level of detail is not shown here, and may not always be necessary.) ***The base rate frequencies for annual probability of initiation shown in Chapter IV-4 are not applicable for seismic loading because the probability of initiation is not the probability given another year of normal operation, but a probability given that the earthquake and settlement have occurred.*** Additional guidance for seismically-induced cracks is provided later in this chapter.

Probabilities assigned to events or conditions are multiplied along each branch's pathway, leading to a joint probability for the particular combination of events or states along that path. Each branch ending in a failure condition contributes to the total failure probability. The individual contributions are summed to yield the annual probability of failure from the earthquake loading.

In case histories, liquefaction has involved significantly more damage to embankments (deformation and cracking) than cases without liquefaction. Therefore, risk from seismic failure modes is frequently evaluated separately on branches with and without liquefaction, rather than, for example, a single tree for internal erosion through cracks that is applied to both with and without liquefaction.

The example event tree shown above is rather simple in appearance, but it may involve complex calculations outside the tree. This might include estimates of post-earthquake remnant freeboard and the probability of breach as a function of freeboard. The required level of complexity has to be judged case by case. If instability could occur in either the upstream direction or the downstream direction (or both), a more complex tree may be needed. This might include separate estimates of liquefaction probability under the upstream slope, the downstream slope, both, and neither. It may not be possible to treat upstream and downstream liquefaction as independent events, because geologic similarity of materials would cause them to be at least somewhat correlated. Issues related to estimation of probability of liquefaction (e.g., joint probabilities,

independence, and correlation) must be considered for liquefaction and shear strength loss, for the upstream slope and downstream slope separately.

The example event tree shows the loading conditions as ranges of PGA and reservoir level. PGA is not always the best seismic loading parameter to use in the event tree because liquefaction potential and deformation are sensitive to other factors, such as the duration of strong shaking and the frequency content of the ground motion. For example, a PGA of 0.15g may have a 1,000-year return period, but it could result from either a nearby crustal earthquake with a small magnitude and short duration or from a much larger but distant subduction zone earthquake. The latter is more likely to cause liquefaction, and with or without liquefaction, more deformation would be expected because it would produce many more cycles of shaking. Quite possibly, a small, nearby earthquake would not cause liquefaction and would cause only minimal deformation, but a subduction zone earthquake with the same PGA would cause widespread liquefaction and large deformation. It may be necessary to partition the loading by both PGA and magnitude, or to employ other measures of loading. It is therefore important to understand the source characteristics. PGA hazard often consists of components from sources of different types, with different magnitudes and ground-motion frequency content.

As discussed in Chapter I-5 Event Trees, partitioning of the load should consider how the behavior of the embankment would vary with the loading. Within a given increment of load, there should not be a wide range of expected behavior or of probability of some event like liquefaction. The steps to evaluate the event tree are described in more detail below.

D-8.7 Loading Conditions

D-8.7.1 Seismic Loading

Larger accelerations and longer durations are generally expected to occur less frequently than small accelerations. Earthquakes can occur randomly within a region of similar seismic activity or be associated with an identified seismogenic fault source. Regional slip rates determine potential earthquake frequency on faults. Statistical models determine earthquake frequency where not associated with a fault. Seismic hazard is typically provided as a return period or an annual exceedance probability for peak horizontal acceleration or in spectral acceleration form at

specified periods or period ranges. Acceleration time-history records thought likely to represent specified return period ranges are also used. For the evaluation of liquefaction, the seismic hazard curves need to be deaggregated to determine the magnitude of the earthquakes that have the most contribution to a particular acceleration increment. The USGS has a number of useful tools available on their website for estimating the seismic loads and frequencies. The selection and description of seismic load ranges is covered in the Chapter II-3 Probabilistic Seismic Hazard Analysis and Chapter I-5 Event Trees.

D-8.7.2 Reservoir Loading

Seismic potential failure modes are also a function of the reservoir level at the time of the earthquake. The system response will have to be developed as a function of both the seismic loading and the reservoir loading. The range of reservoir loadings should go from the minimum normal pool to the maximum controllable level, since the duration of storage over an uncontrolled spillway or above designated flood storage with a gated spillway is generally pretty short. USACE will often develop a range of reservoir loadings from the minimum normal pool to the PMF elevation or dam crest for flood control dams using a stage-duration relationship. The frequency associated with the reservoir loading should be based on the stage-duration curve developed for the project. This will give the percent of time the pool is expected to be above a certain elevation.

D-8.8 Site Characterization

D-8.8.1 Continuity of Liquefiable Materials

The first item to be addressed is the likelihood that a continuous layer or zone of potentially liquefiable material exists within the dam or foundation. This may be explicitly included as a node in the event tree. While simple in concept, estimating the likelihood for continuity requires significant insight. It is typically based on exploratory information and knowledge of the geologic and dam construction processes. For example, the extent of a potentially liquefiable foundation layer is formulated from what is known about the foundation. If the foundation is composed of lacustrine deposits or if the embankment contains hydraulic fill, there would be reason to believe soil properties identified for a layer would in general be laterally continuous. The same may not be true for alluvial stream deposits.

Soil property data, such as Standard Penetration Tests (SPT), Becker-Hammer Penetration Tests (BPT), Shear Wave Velocity Tests (SWV), and Cone Penetrometer Tests (CPT) can provide insights into the potential for a continuous layer. ***In this regard, the data should be reviewed looking for a continuous low strength layer and not as a population lumped together for statistical analysis.*** The extent of the loose layer can often be constrained to within some limits from this type of data. Then, it becomes a matter of judging the likelihood that the identified layer is continuous enough to lead to a stability problem if it were to liquefy. All field testing should be carefully reviewed to assure that borehole drilling methods or testing methods did not cause significant disturbance that may alter the interpretation of the data. It has been found that improper control of drilling fluid pressures has resulted in borehole heave, and thus subsequent testing indicated false interpretations of low density zones. Whenever very low blow counts are recorded under dams with significant confining pressure, the field drilling and testing methods should be closely scrutinized. Construction photographs, especially of trench excavations, should be used to help assess the continuity and character of the foundation materials.

Typically, continuity parallel to the dam axis of 1 to 2 times the dam height is needed to adversely affect stability without significant three-dimensional effects contributing to stability. If the continuity transverse to the dam axis underlies most of the dam slope, it is probably of sufficient continuity to affect slope stability. Shorter transverse continuity can also affect slope stability depending on the geometry and strength. Slope stability analyses incorporating post-liquefaction shear strengths can be useful in determining how far low-strength materials need to extend beneath a slope before stability becomes an issue.

When there are few of the in situ tests normally used to evaluate liquefaction potential at a site, it has been common to first estimate the likelihood of continuity, and then estimate the likelihood that the zone thought to be continuous can liquefy. When there are many in situ tests, it is common to estimate a range of values for some material property (e.g., SPT blow count or shear strength) related to liquefaction and thought to be “representative” of a zone under the embankment slope that extends laterally 2 to 3 times the height of the embankment. Again, the “representative” value should be judged based on a critical evaluation of the geology and in situ test data, taking care to look for weak zones which have continuity. It is generally best to avoid

equating “representative” with a statistical average of the deposit as a whole. Instead, look for an average strength or blow count over a surface drawn through the weakest depths at each drillhole location (supplemented by geologic judgment regarding which materials should be included in the average). A frequent mistake is to take the average of all of the available SPT blow counts in a given geologic unit, regardless of whether the unit appears to have a recognizable low-blow count zone of sufficient extent. Another mistake is to take the average of all of the available data in a unit when borehole spacing is much greater than 2 to 3 times the dam height. In this case, a single low-blow count interval in a single borehole could be significant.

D-8.8.2 Other Parameters

Along with determining the representative normalized blow counts required to assess liquefaction, many other parameters need to be determined to help evaluate the dam. This includes strengths for non-liquefiable materials, densities, piezometric levels, etc. Additionally, if site response analysis will be done, shear wave velocity measurement may be required. Regional or site-specific fault studies may be appropriate when active faults are present on or near the dam site.

D-8.9 Likelihood of Liquefaction

Estimating the likelihood of liquefaction for any given zone or layer depends on several factors and requires computations outside of the event tree. It is not the intent of this section to provide a detailed discussion of liquefaction evaluation. See the embankment dam draft seismic design standard (Reclamation 2001), USACE’s Draft EC 1110-2-6001 Seismic Analysis of Embankment Dams, Seed et al. (2003), Idriss and Boulanger (2008, 2010), Bray and Sancio (2006), and Boulanger and Idriss (2004) for more information.

Several analyses need to be conducted before the risk assessment occurs. The cyclic shear stresses or a_{max} will need to be determined from either a site response analysis or simplified Seed analysis. If time histories are readily available, a site response analysis is preferred. The cyclic stress ratio will need to be calculated for each particular load level, at key locations beneath the dam. In addition, raw blow count data will need to be normalized and corrected for fines content. If CPT or shear wave velocity data is to be used, that information must be reduced and

normalized. See Idriss and Boulanger (2008, 2010) or Seed et al. (2003) for a discussion of these methods.

Bray and Sancio (2006) report on how soils of differing plasticity index demonstrate liquefaction susceptibility. Boulanger and Idriss (2004, 2008) provide additional guidance on liquefaction and post-liquefaction behavior of fine-grained soils.

Probabilistic liquefaction models are all based on statistical regressions using adjusted SPT $(N_1)_{60}$ blow count, fines content (FC) or percent passing the No. 200 sieve, and adjusted cyclic stress ratio ($CSR_{M=7.5,\sigma'v=1atm}$) as the basic input parameters: Liao et al. (1988), Youd et al. (2002), Cetin et al. (2000 and 2004), and Seed et al. (2003). Idriss and Boulanger (2010) is the most recent relationship developed from a thorough, updated re-examination of the case history database and database of cyclic test results for frozen sand samples. It is considered to be a technical supplement to Idriss and Boulanger (2008). The Idriss and Boulanger (2010) probabilistic liquefaction triggering correlation is expressed as follows:

$$P_L\left((N_1)_{60cs}, CSR_{M=7.5,\sigma'_v=1atm}\right) = \left[\frac{\frac{(N_1)_{60cs}}{14.1} + \left(\frac{(N_1)_{60cs}}{126}\right)^2 - \left(\frac{(N_1)_{60cs}}{23.6}\right)^3 + \left(\frac{(N_1)_{60cs}}{25.4}\right)^4 - 2.67 - \ln\left(CSR_{M=7.5,\sigma'_v=1atm}\right)}{0.13}\right]$$

Equation D-8-1

Where

$$CSR_{M=7.5,\sigma'_v=1atm} = 0.65 \frac{\sigma_v}{\sigma'_v} \frac{a_{max}}{g} r_d \frac{1}{MSF} \frac{1}{K_\sigma}$$

Equation D-8-2

Conventional cyclic resistance curves such as those Idriss and Boulanger (2008) and Youd et al. (2001) (the NCEER volume) are frequently treated as if they are deterministic boundaries that preclude liquefaction if the CSR is below the curve. In fact, they are not deterministic (and were

not intended to be); instead, a pair of $(N_1)_{60CS}$ and $CSR_{M=7.5,\sigma'v=1atm}$ lying on the curve has about 15 percent probability of liquefaction.

Where there is not an obvious representative value of $(N_1)_{60CS}$ for a potentially liquefiable deposit, uncertainty in $(N_1)_{60CS}$ can be addressed by creating a probability distribution, either a discrete distribution that appears as branches on the event tree, or a continuous probability distribution that is used in "off-tree" calculations of liquefaction probability. It may be appropriate to examine more than one distribution, depending on the available information. One can also create separate distributions for $(N_1)_{60}$ and FC for off-tree calculation of $(N_1)_{60CS}$. A spreadsheet can then be used to calculate the probability of liquefaction using the $(N_1)_{60}$ and FC distributions.

Boulanger and Idriss (2014) provide an analogous model for finding liquefaction probability from cone penetrometer test (CPT) data.

Once the probability of liquefaction is determined, then the probability of no liquefaction is calculated as one minus the probability of liquefaction.

D-8.10 Residual Shear Strength of Liquefied Soil

An estimate of the residual shear strength of the liquefied materials (S_{ur}) is needed to estimate deformation. Several empirical relationships have been published that correlate residual undrained shear strength of liquefied material with standard penetration test resistance. The most common relationships used in practice include Seed and Harder (1990) as shown in Figure D-8-7 and Idriss and Boulanger (2008) as shown in Figure D-8-8. The primary difference between the two is that the Seed and Harder relationship provides S_{ur} as a function of blow count, but Idriss and Boulanger relationship provides the ratio S_{ur}/σ'_{vo}, where σ'_{vo} is the pre-earthquake vertical effective overburden stress. For a given value of $(N_1)_{60}$, S_{ur} tends to be higher with higher fines content, FC. Both of the relationships mentioned require $(N_1)_{60}$ to be adjusted by adding an adjustment that is a function of FC, shown below in Table D-8-1, to find the clean-sand equivalent blow count $(N_1)_{60cs\text{-}Sr}$. This adjustment is somewhat different from the adjustment used to find $(N_1)_{60cs}$ for liquefaction triggering.

Within the very limited case history database, most instances of flow liquefaction have occurred at fairly shallow depths (i.e., low effective overburden pressure), and none had an $(N_1)_{60\text{-}cs}$ value above 14. It is likely that the lack of embankment flow liquefaction cases for the medium to high blow count materials is related to the fact that high blow count materials are dilative, and the medium blow count materials which may be initially contractive become dilative with strain. (The lack of those case histories might also result in part from a lack of good "tests," where steep slopes with somewhat higher blow counts were subjected to loading severe enough to cause liquefaction.) The Seed and Harder (1990) relationship does not allow for any beneficial effects from higher effective overburden stress, common beneath large embankment dams. Idriss and Boulanger (2008) used blow counts and strength estimates from both Seed and Harder and Olson and Stark (2002) to develop their relationship for shear strength ratios. For extrapolation beyond the limits of available data, they present two different curves as shown in Figure D-8-8. The lower curve is for use where there is potential for settlement of soil particles and upward migration of water-filled voids to create a very weak fluidized zone below a less pervious layer. The upper curve is for situations without that potential, because there would be free upward drainage of the water expelled by settlement. When it isn't obvious which is most nearly correct, it may be appropriate to consider both probabilistically. The two curves are essentially the same within the limits of available data.

Table V-6-1. Blow Count Corrections to Obtain Clean Sand Equivalent (Seed 1987)

Fines Content (percent)	Blow Counts (bpf) added to $(N_1)_{60}$
10	1
25	2
50	4
75	5

Gillette (2010) reviewed the various relationships in an attempt to determine the most appropriate correlation between overburden and blow count. The strength-ratio approach appears to work better at higher effective overburden stresses (exceeding 1,000 to 1,400 psf) than at lower ones. For medium-density soils (dense enough to dilate at larger strains after initial liquefaction), the strength ratio is thought to be the most realistic model, as the shearing resistance increases with larger strain and becomes a large fraction of the drained strength. However, care must be taken in selection of undrained residual shear strength from such correlations given very limited data at higher effective overburden stresses and within alluvium as opposed to other materials that have liquefied.

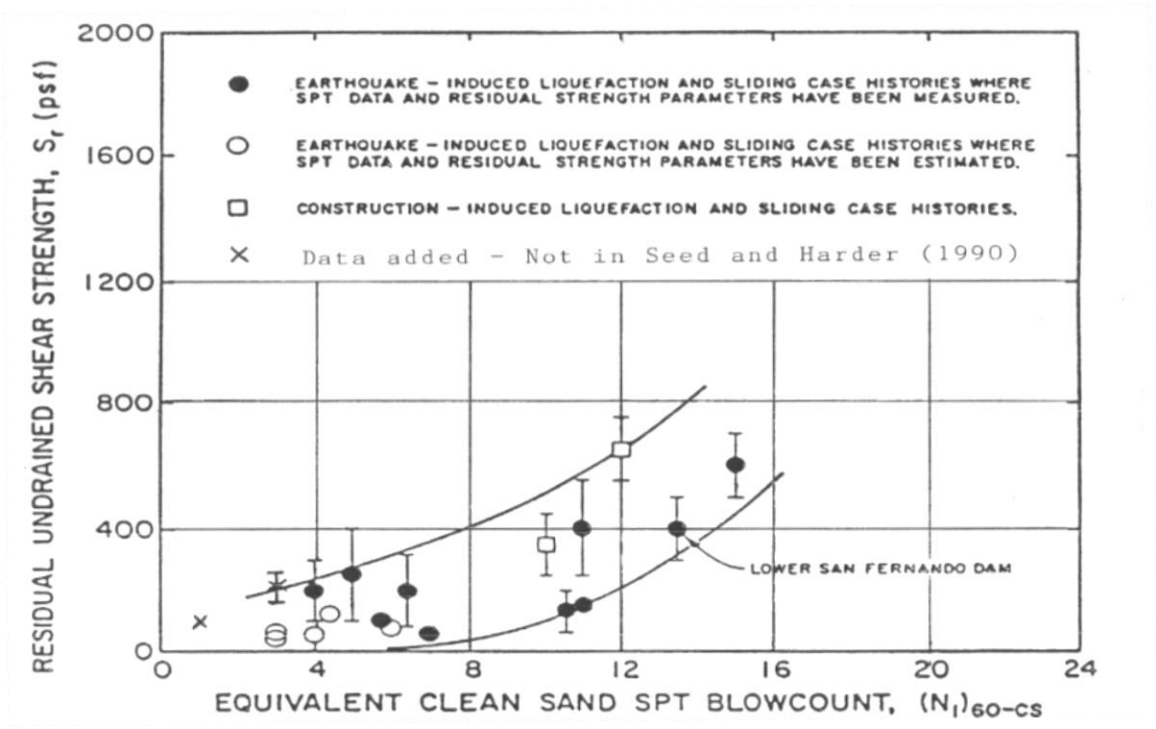

Figure D-8-7. Residual Undrained Shear Strength
(adapted from Seed and Harder 1990)

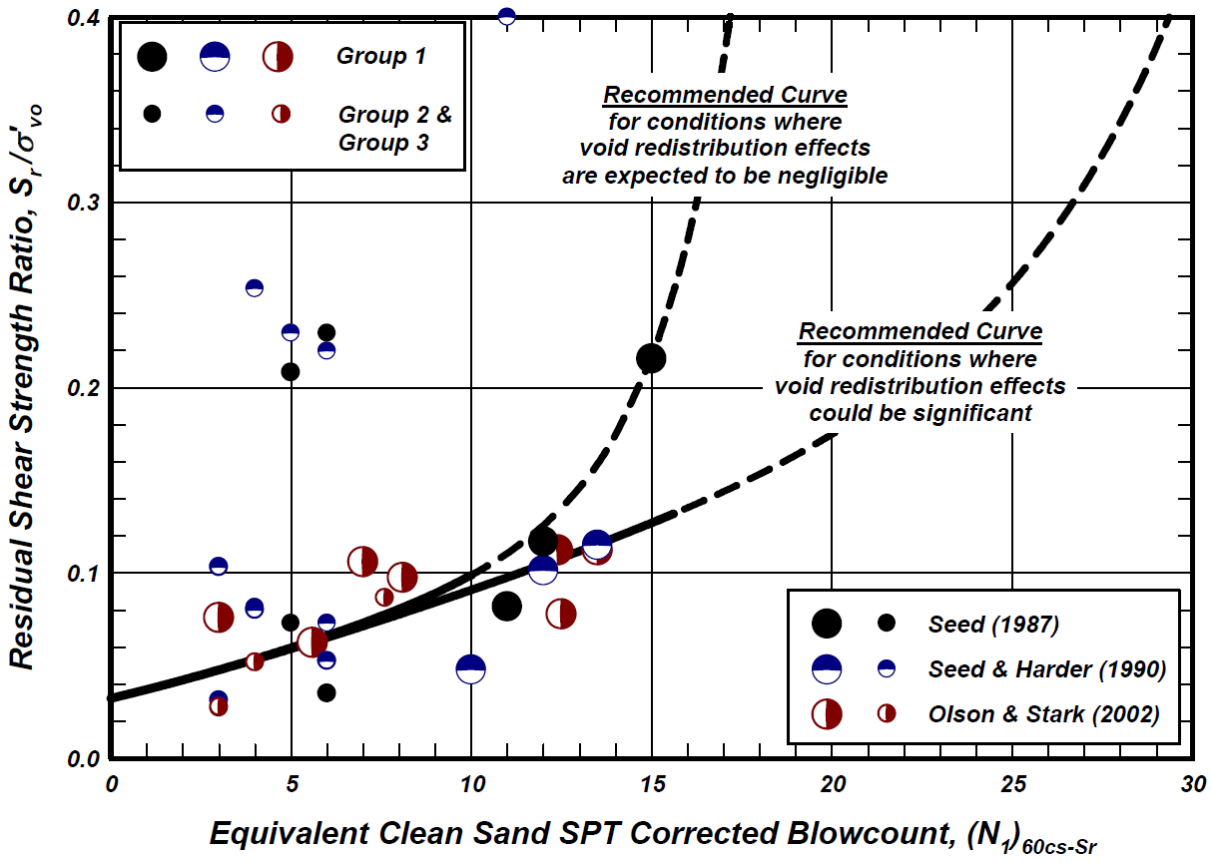

Figure D-8-8. Normalized Residual Shear Strength Ratio of Liquefied Soils (Idriss and Boulanger 2008)

D-8.11 Embankment Deformation

There are numerous methods used to estimate deformations of embankments in response to seismic loading. Unfortunately none of the methods, (including rigorous models) have been proven to accurately predict actual deformation shape and magnitudes. The risk assessor must be familiar with the assumptions and limitations of the methods used to estimate the embankment deformation and apply significant judgment when assessing the probability associated with deformation-related potential failure modes. Simplified methods should be used first. If an evaluation using one of the simplified methods results in an estimated annual probability of failure or annualized incremental life loss that exceeds risk guidelines, more refined studies are probably justified. This requires detailed FLAC analyses to estimate the loss of freeboard due to various seismic loads. Typically, enough FLAC analyses are run to develop curves (high, median, and low) for freeboard loss as a function of residual undrained shear strength of the

liquefied layers or zones. Team judgment incorporating model uncertainty is also included in the development of the curves.

D-8.11.1 Empirical Deformation (No Liquefaction Occurs)

If liquefaction does not occur, movements that occur within the dam body without distinct signs of shearing displacement can lead to deformation that exceeds the available freeboard. Swaisgood (1998, 2003, 2014) examined case histories of seismic-induced settlement and mass deformation where the earthquake shaking causes embankments to settle downward and sidewards, towards the deepest center portion of the valley, and then spread upstream and downstream away from the dam axis. In the Swaisgood empirical methodology, the crest settlement is expressed as a percentage of the total embankment height and foundation thickness, as shown in Figure D-8-9. The crest settlement (given that no liquefaction occurs) is given as a function of peak ground acceleration (PGA) and surface wave magnitude (M_s) as shown in Figure D-8-10. ***The incident database does not contain any cases with PGA greater than 0.7g or normalized settlements greater than 5 percent. However, some incidents involving liquefaction were included in the database as shown in Figure D-8-11: Hebgen Dam (1959), Upper San Fernando Dam (1971 and 1994), and Masiway Dam (1990). Austrian Dam (1989) did not experience liquefaction but had other issues like poor compaction and an existing slide left in place in one abutment. If these cases are excluded, the incident database does not contain any cases with normalized settlements greater than 1 percent.***

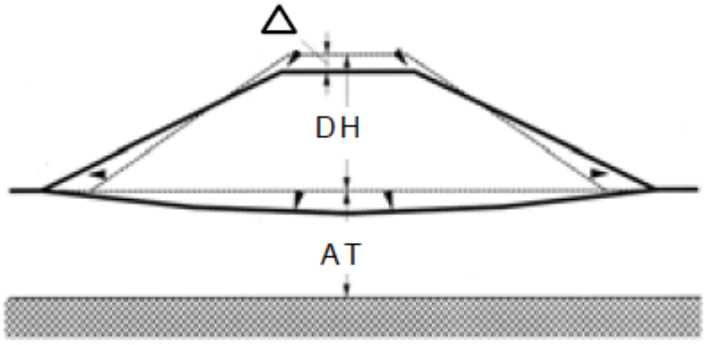

$$NCS = \frac{\Delta}{DH + AT} \times 100\%$$

Figure D-8-9. Crest Settlement (Swaisgood 2014)

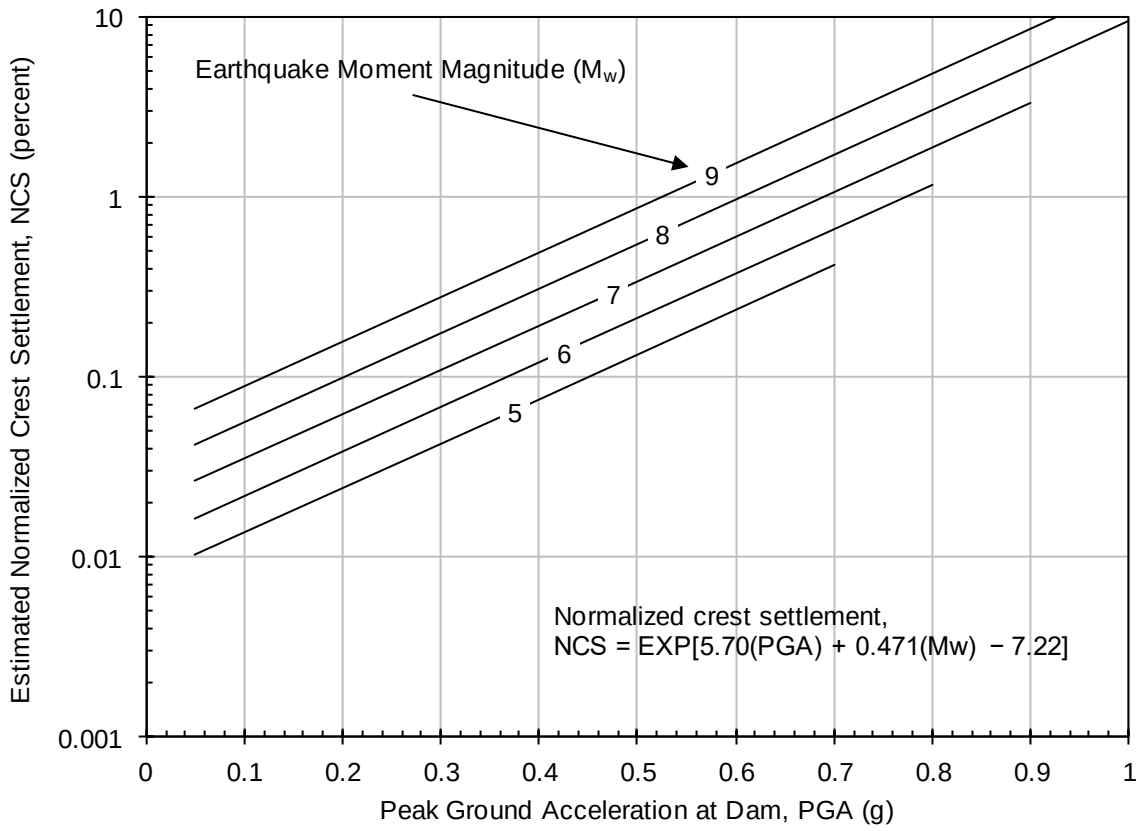

Figure D-8-10. Estimated Normalized Crest Settlement

(Replotted from Swaisgood 2014)

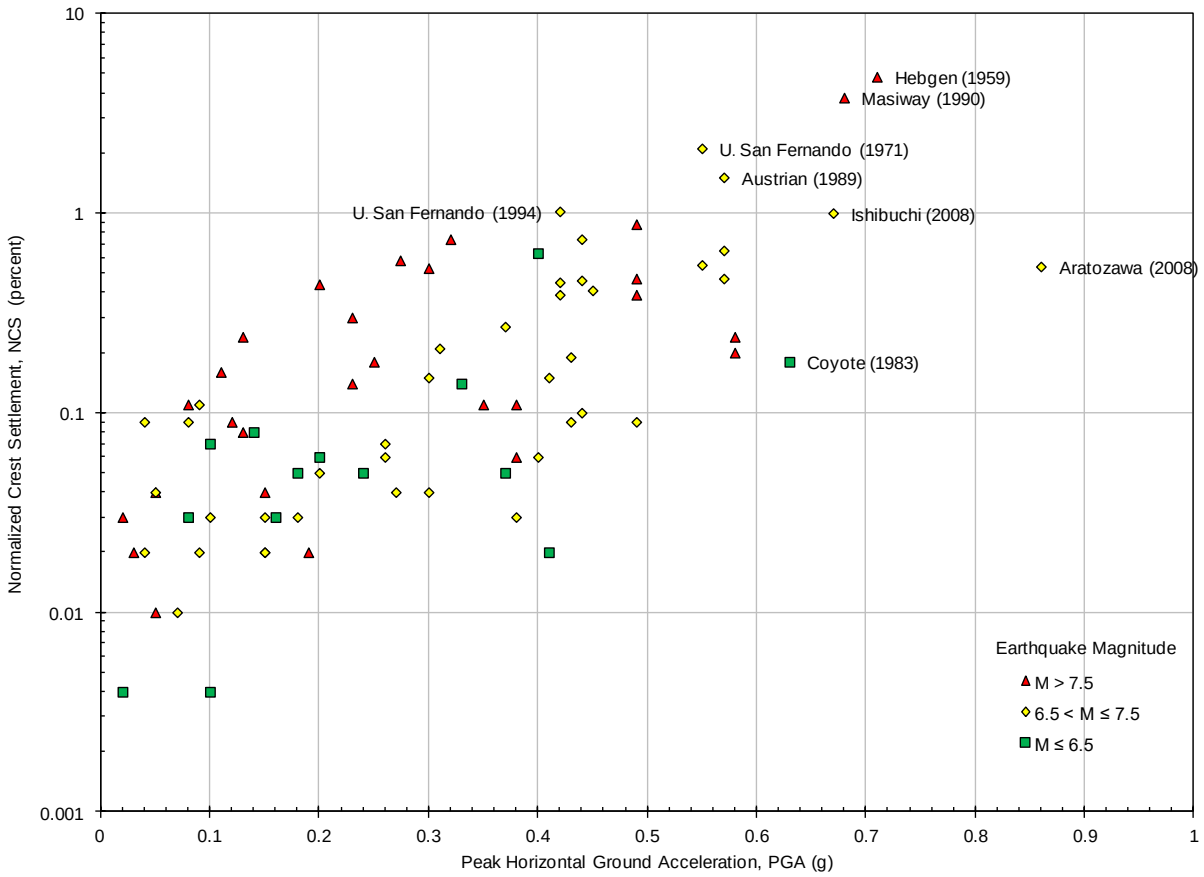

Figure D-8-11. Estimated Normalized Crest Settlement
(Replotted from Swaisgood 2014)

D-8.11.2 Simplified Dynamic Slide Mass Deformation

Newmark (1965) developed a method for estimating the displacement of a slide mass due to dynamic shaking based on the assumption that permanent displacement occurs when the dynamic stress exceeds the shear resistance along the sliding mass. This method has been modified and updated by others including: Makdisi and Seed (1978), Watson-Lamprey and Abrahamson (2006), and Bray and Travasarou (2007). Limitations include:

- Deformation is only assumed to occur only along the sliding surface and not as shear strain throughout the embankment.
- Deformation assumed to only occur during the shaking
- Only valid for non-liquefied embankment and foundation materials

D-8.11.3 Post-Earthquake Stability Analysis

Limit equilibrium slope stability modeling can be used to assess the likelihood that the embankment will have significant deformation and discern a very approximate value for maximum crest deformation when the embankment slope has a factor of safety less than 1. The factor of safety of a dam slope should be determined given the potentially liquefiable zones are at their residual shear strength. The failure surfaces evaluated should only be for significant slide planes that would influence the performance of the dam and lead to potential breach. If the factor of safety is determined to be in the 1.2 to 1.3 range, it is likely that the embankment will not develop significant displacement. If the factor of safety is less than or equal to 1.1, large movements are much more likely. With enough movement, the reservoir may be able to overtop the remnant embankment. If not, the reservoir would be held back only by the remnant embankment behind the sliding mass. Essentially, this remnant of relatively undisturbed embankment material would provide the highest remaining barrier to uncontrolled reservoir release. The peak of the undisturbed remnant could be used to assess the likelihood of overtopping. Figure D-8-12 shows a series of circular and wedge-shaped failure surfaces analyzed using a limit equilibrium method. Figure D-8-13 shows the same cross section modeled using FLAC. The deformation arrows are absent in Figure D-8-13 on the downstream slope at a point where the Figure D-8-12 shows a failure surface that has a factor of safety of 1.12. The FLAC analysis shows highly deformed material remaining above the elevation of the peak of the undeformed section. An estimate of the remnant crest can be made by assuming that all of the slide mass moved below the scarp intersection with the embankment. The likelihood of attaining a safety factor along such a surface less than this can be estimated using reliability analysis (see Chapter I-7 Probabilistic Stability Analysis) using a software program like SLOPE/W which can be run in a probabilistic mode. In general, the process is very similar to performing a conventional stability analysis, but instead of defining the input parameters as discrete values, they are characterized as random variables with a probability distribution. A Monte Carlo simulation is used to determine the probability of obtaining a factor of safety less than 1.0.

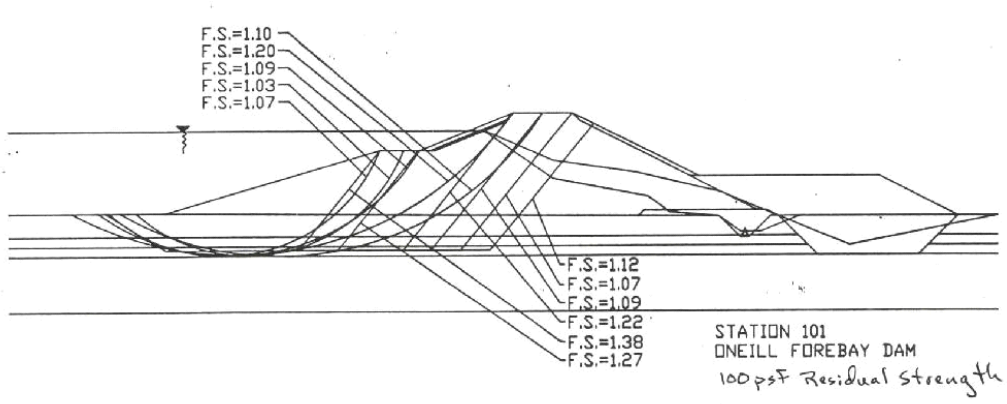

Figure D-8-12. Results of Post-Earthquake Limit-Equilibrium Slope Stability

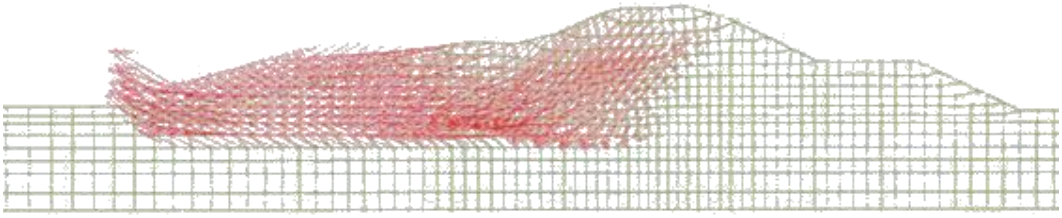

Figure D-8-13. Results of Finite Difference Model

D-8.11.4 Simplified Post-Earthquake Deformation Screening

FMSM (2007) performed a parametric study to develop simplified equations for post-earthquake deformation. USACE may use the results along with other factors for a quick screening-level assessment only, but Reclamation does not. It was assumed that the post-earthquake static deformation is the primary contributor and deformation during shaking was not evaluated. A parametric analysis of over 20,000 cases was performed using FLAC. Six variables were considered: height of embankment (H_{emb}), thickness of liquefied foundation soil (H_{liq}), side slopes (m_{side}), normalized depth of pool (h_{pool}) , shear strength ratio of embankment soil (r_{emb}), and shear strength ratio of liquefied foundation soil (r_{liq}). Of the 20,000 cases evaluated only 8,612 (43 percent) resulted in a valid converged solution. Solutions were not obtained for cases where the embankment was unstable before liquefaction, and convergence was not obtained for cases with severe localized distortion. ***Only the valid converged cases were used to develop a regression equation to estimate deformation.*** The regression equation for crest deformation represents the difference in the elevation between the initial embankment crest and the highest

valid grid point on the surface of the deformed embankment computed in the FLAC model. For screening, the crest deformation of an embankment given liquefaction occurs can be estimated using the following expression:

$$\log_{10}(\Delta) = -6.399 \cdot H_{emb}^{-1} - 0.6023 \cdot \log_{10}(r_{emb}) + 1.581 \cdot \log_{10}(m_{side}) - 4.689 \cdot h_{pool} H_{emb}^{-1} + 0.9123 h_{pool}^{3} - 6.256 \cdot H_{liq}^{-1} - 8.428 \cdot r_{liq} + 2.620$$

Equation D-8-3

The reported R^2 value for the regression equation is 0.803. Valid ranges are specified by FMSM (2007) for the input parameters and irregular or asymmetrical embankment cross sections. The variables are defined in Figure D-8-14. Only basic geometries can be evaluated with this method. To use this tool with multiple layers or complex geometries, an equivalent simplified cross section must be developed, as described in FMSM (2007). The loss of freeboard needs to be compared to the reservoir elevation at the time of the earthquake.

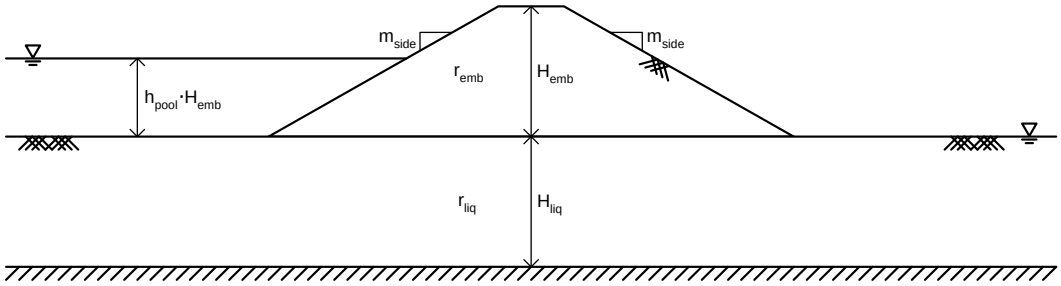

Figure D-8-14. "Generalized" Cross Section (FMSM 2007)

D-8.11.5 Numerical Post-Earthquake Deformation

If the team has an experienced modeler available, then performing a post-earthquake static deformation analysis using a computer program like FLAC can be very valuable. The materials that are potentially liquefiable are modeled at their residual undrained shear strengths. Only gravity loading is applied, and the deformed shape and displacement magnitudes are determined. This analysis neglects the potential deformation that could occur during the shaking. Many observations of embankment instability from seismic loadings have indicated that most of the deformation actually occurs after the shaking stops. This analysis is much less complicated, when compared to the issues of modeling the deformation during dynamic shaking, and are generally considered more reliable.

D-8.11.6 Numerical Dynamic and Post-Earthquake Deformation

The computer program FLAC can also be used to analyze seismically-induced deformation. FLAC is a two-dimensional explicit finite-difference program. This program can be used to simulate the behavior of structures built of soil, rock, or other materials that may undergo plastic flow when their yield limits are reached. Materials are represented by zones and regions that may be shaped by the user to conform to the physical structure being modeled. Each zone is assumed to behave according to a prescribed linear or nonlinear stress/strain law in response to applied forces or boundary constraints. The represented material can yield and flow, and the grid can deform and move with the material being represented. However, caution and experience are needed when using such sophisticated nonlinear computer programs to ensure the results are reasonable. The models should be thoroughly tested, validated, and verified to ensure reasonable performance. Parametric evaluations should be performed to make sure the model is producing results that intuitively seem to match the expected behavior. The results of this testing should be documented so that those reviewing the results of the analyses will have as much confidence as possible in the results. Model uncertainty can be included in the probability estimates rather than strictly relying on the output numbers (e.g., to account for three-dimensional effects if two-dimensional models were used).

Deformation can result from slope instability under gravity loading alone. If an earthquake can trigger liquefaction, pore water pressure increases reduce shear strength, and the slope might become unstable. After liquefaction triggering, a slope can continue to deform even though the earthquake shaking has ceased if the static factor of safety is less than 1. Should liquefaction initiate early in the earthquake, continued shaking provides inertial forces that add to deformation. Modeling experience using FLAC has shown that when the static factor of safety is less than 1, the dynamic deformation portion is typically a small fraction of the total deformation. Intuitively, the dynamic component will be more significant for earthquake acceleration records of long duration, particularly when the earthquake provides strong accelerations with long periods (as indicated by high spectral acceleration for long periods, such as 1 second).

Resource constraints usually dictate that FLAC results are generated for a limited number of loadings and assumed initial conditions. For the example in Figures D-8-15 and D-8-16 below, a foundation layer beneath an embankment slope was assigned residual shear strength values of 50, 100, and 200 psf. Gravity loading alone produced the deformation values labeled "Static." A relatively strong earthquake was responsible for the additional deformation labeled "Dynamic." Connecting the six model point-estimates with lines, as shown in Figure D-8-15, is reasonable. One could easily analyze the model with additional parameter assumptions to fill in the spaces between previous runs. Likewise, extrapolating the lines to the right, as shown in Figure D-8-16, is appropriate, and we would expect verification with additional analysis for higher shear strength values. Extrapolation to the left as shown in Figure D-8-16 is much more problematic, especially if the post-earthquake static factor of safety approaches or falls below 1.0. In that case, there is a transition between two general types of behavior, dynamic deformation occurring only during strong shaking, and gravity-driven slope instability. Limit-equilibrium slope stability (SLOPE/W or similar program) may be necessary before extrapolating.

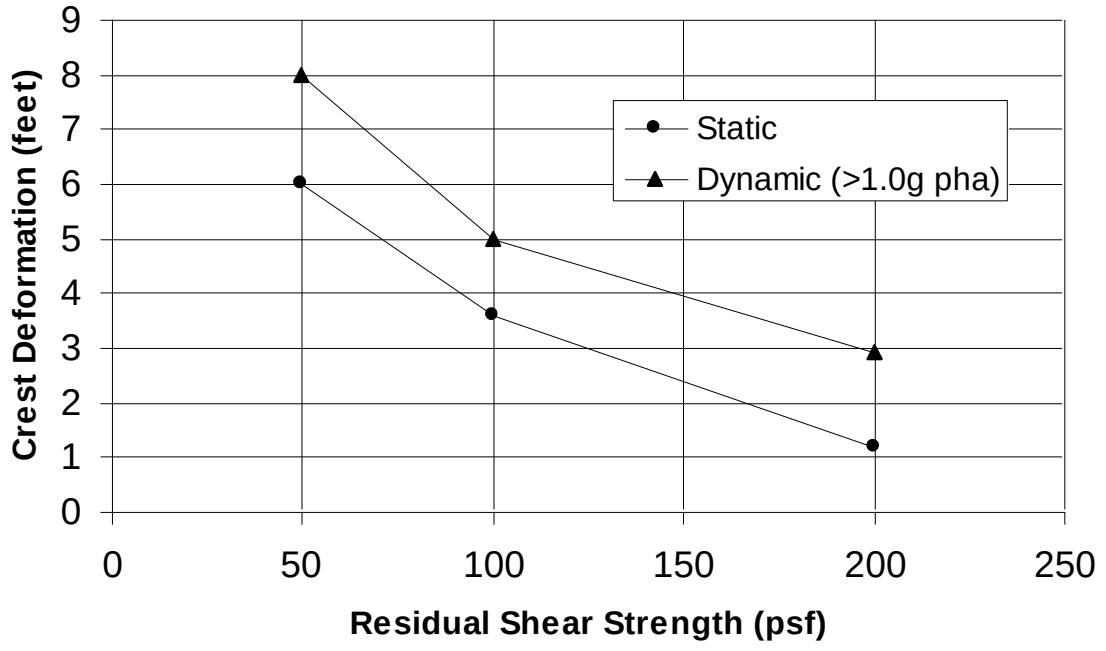

Figure D-8-15. FLAC Results for 6-Point Static/Dynamic Model

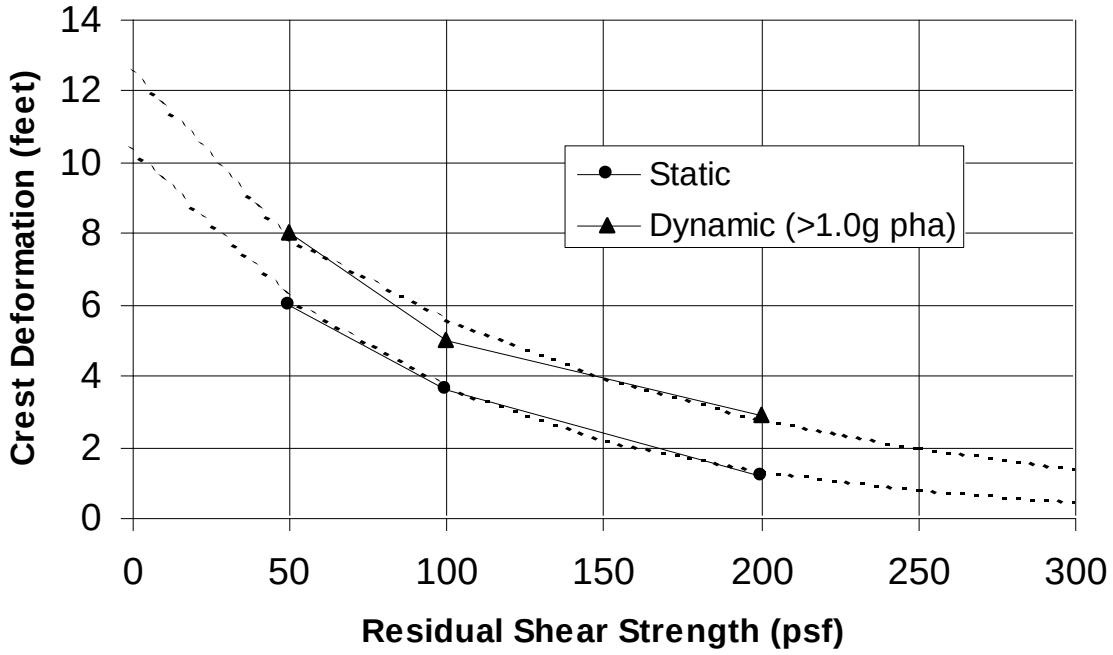

Figure D-8-16. Extrapolated FLAC Results from 6-Point Static/Dynamic Model

D-8.12 Overtopping (Deformations exceeding Freeboard)

The probability of overtopping is typically estimated by developing curves of expected deformation. For example, the team may estimate the range of absolute minimum crest settlement, reasonable minimum settlement, best estimate or median settlement, reasonable maximum settlement, and absolute maximum crest settlement. These values then form a probability distribution of crest settlement for the strength loss value assumed to result from liquefaction or cyclic failure. If the reservoir remains relatively constant, the deformation curves represent the likelihood of losing a particular amount of freeboard, which can be compared to the freeboard prior to the earthquake in order to assess the likelihood of a breach. If the reservoir fluctuates considerably, the operations cycles are reviewed to get a feel for the percent of time the reservoir is above a threshold level for seismic failure modes to initiate using a pool-duration relationship can be used to represent the coincident pool at the time of the earthquake. The seismic hazard curve performs the annualization, and the reservoir's stage-duration curve provides the fraction of time that a reservoir level is equaled or exceeded.

In some cases, branches for the continuity of liquefiable materials, strength loss, and deformation exceeding freeboard are combined by considering the probability of a given strength scenario,

and the resulting deformations given each strength scenario. Specifically, the first two probabilities (probability of continuity and probability of strength loss) are instead phrased as the probability that a given strength will result from a given increment of earthquake loading. This is particularly useful when the team has developed deformation models for several different strength scenarios. The strengths assigned in these scenarios are meant to model a likely range of values and include reasonable upper and lower bounds. For example, if Newmark and/or FLAC analysis have been performed for three different strength assumptions, the team estimates the likelihood of each of the three strength assumptions, with the sum of the three probabilities equal to 1.0. Expected deformation curves for each of the three strength scenarios can then be developed as described above. This approach is useful in allowing teams to reflect the (sometimes considerable) uncertainty in estimating the strength loss (and corresponding deformations) that will result from earthquake shaking.

D-8.13 Internal Erosion through Cracks

If the embankment and foundation do not liquefy or if the freeboard is not completely lost through seismic deformations, the dam will not fail due to overtopping (or rapid erosion of the severely damaged dam crest), but there is still the potential for a slower internal erosion through cracks in the embankment, typically in the crest and upper portions of the dam. Fell et al. (2008) include considerations for internal erosion through seismically-induced cracks based in part on observed damage to embankment dams following large earthquakes. The primary goal is to determine how deep the embankment is likely to crack and how open the cracks are likely to be below the reservoir surface. Once this is determined, the likelihood of internal erosion is assessed in a similar fashion as for flood loading.

The methodology of Fell et al. (2008), described below, can be used as a tool to assess the likelihood of a crack due to earthquake shaking. The first step in the procedure is to determine the damage class from Figure D-8-17 or D-8-18. This typically requires deaggregation of the seismic hazard to determine the magnitudes of the earthquakes that contribute most to the hazard at various peak horizontal ground accelerations. If liquefaction occurs, Damage Class 3 or 4 can be assumed, depending on the severity of the estimated liquefaction. Fell et al. (2008) suggest assuming Damage Class 4 if flow liquefaction occurs and Damage Class 3 if liquefaction occurs

but it is not flow liquefaction. A Damage Class is determined for each earthquake load partition. It is often desirable to develop a separate event tree to evaluate internal erosion through cracks (as opposed to tacking it on to the end of the liquefaction tree at the non-breach nodes). If a separate tree is developed, care must be taken in combining these risks with liquefaction overtopping risks (and other seismic risks), as discussed in Chapter I-8 Combining and Portraying Risks (common-cause adjustment) so as to not assign a combined conditional failure probability that is too high for a given load range. Given the Damage Class, determine the likely settlement as a percentage of dam height from Table D-8-2. Cracking begins at the new elevation of the crest after seismically-induced settlement and extends downward from there.

The probability of transverse cracking and the likely crack width at the crest can be estimated from Table D-8-3, which shows the range of values suggested in Fell et al. (2008). Given the crack opening at the crest, the crack width at various depths below the crest and the probability of initiation can be estimated using the procedure described in the Chapter IV-4 Internal Erosion Risks for Embankments and Foundations.

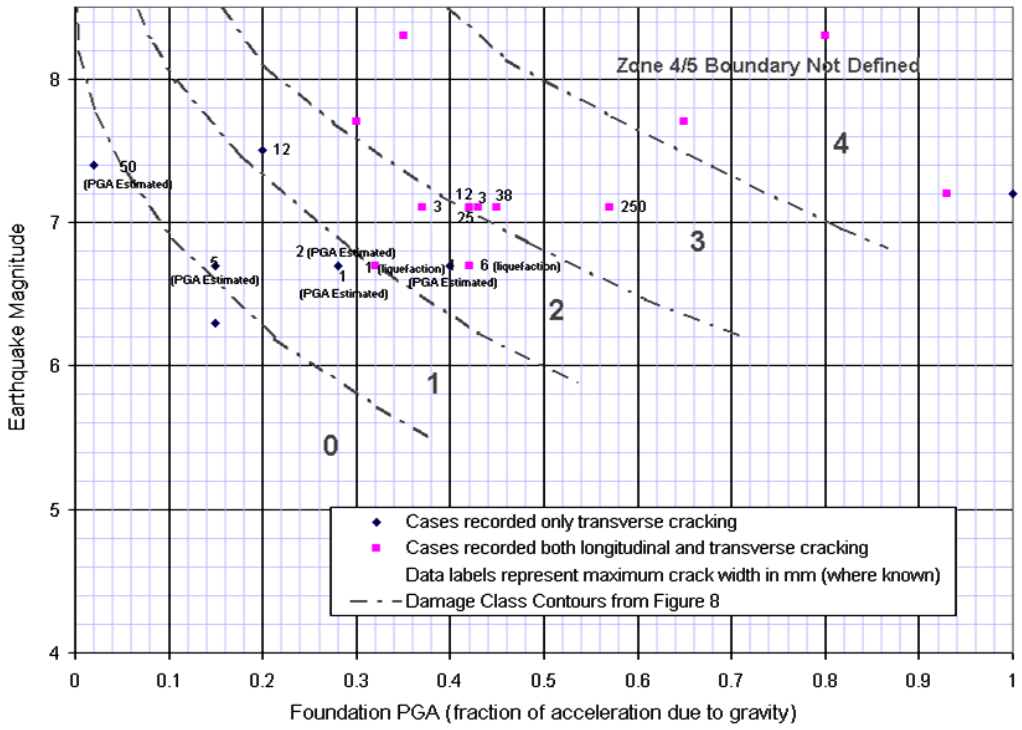

Figure D-8-17. Incidence of Transverse Cracking for Earthfill Dams (Pells and Fell 2002)

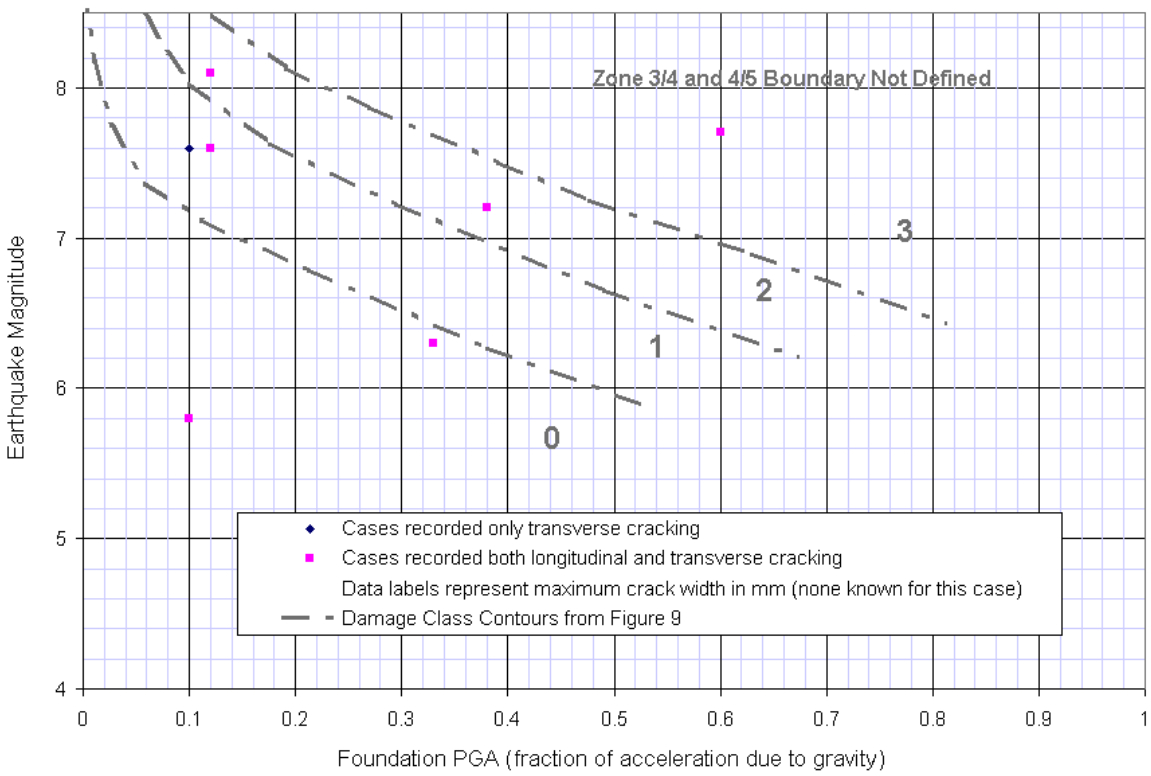

Figure D-8-18. Incidence of Transverse Cracking for Earthfill and Rockfill Dams (Pells and Fell 2002)

Table D-8-2. Damage Classification System (Pells and Fell 2002)

Damage Class		Maximum Longitudinal Crack Width [(1)] (mm)	Maximum Relative Crest Settlement [(2)] (percent)
Number	Description		
0	No or Slight	< 10	< 0.03
1	Minor	10 to 30	0.03 to 0.2
2	Moderate	30 to 80	0.2 to 0.5
3	Major	80 to 150	0.5 to 1.5
4	Severe	150 to 500	1.5 to 5
5	Collapse	> 500	> 5

Notes: (1) Maximum likely crack width is taken as the maximum width of any longitudinal crack that occurs.

(2) Maximum relative crest settlement is expressed as a percentage of the structural height.

Table D-8-3. Probability of Transverse Cracking (Fell et al. 2008)

Damage Class		Probability of Transverse Cracking	Maximum Likely Crack Width at the Crest (mm)
Number	Description		
0	No or Slight	0.001 to 0.01	5 to 20
1	Minor	0.01 to 0.05	20 to 50
2	Moderate	0.05 to 0.10	50 to 75
3	Major	0.2 to 0.25	100 to 125
4	Severe	0.5 to 0.6	150 to 175

D-8.14 Foundation or Reservoir Fault Displacement

Where an active fault or fault capable of coseismic displacement exists in the foundation of a dam, offset along the fault can cause cracking of the embankment and/or conduits passing through the dam. Since each dam and geometry is unique, a site-specific event tree needs to be developed to evaluate this on a case-by-case basis. The loading in this case involves fault offsets of various magnitude ranges and their associated probability. Input from Quaternary geologists specializing in fault and seismic source characterization is typically needed to develop this input. An event tree is developed to describe the specific potential failure mode being evaluated. Nodes

on the tree would include all of the component events required to cause failure of the dam by this mechanism, and their likelihood. This would include, for example, the likelihood of a through-going crack given some amount of fault offset, or of the embankment filter being disrupted, given that the through-going crack has formed.

Bray et al. (2004) provides an analytical method for preliminary estimates of the height of the shear rupture zone in saturated cohesive soils overlying a bedrock fault displacement based on field observations and physical model experiments. The results indicated that propagation of the shear rupture zone in the overlying soil at a specific bedrock fault displacement depends primarily on the clay's axial failure strain, as shown in Figure D-8-19, where the height of the shear rupture zone in the clay overlying the bedrock fault has been normalized with the magnitude of the vertical base displacement. The rupture zone propagates farther in saturated clayey materials that exhibit brittle stress-strain behavior (i.e., low values of failure strain). The orientation of the shear rupture zone through the soil depended largely on the orientation of the underlying bedrock fault plane. The final shear rupture zone in the clay tended to follow the projection of the bedrock fault plane, although there was a tendency for the rupture zone to increase in dip as the rupture zone approached the ground surface and to widen slightly.

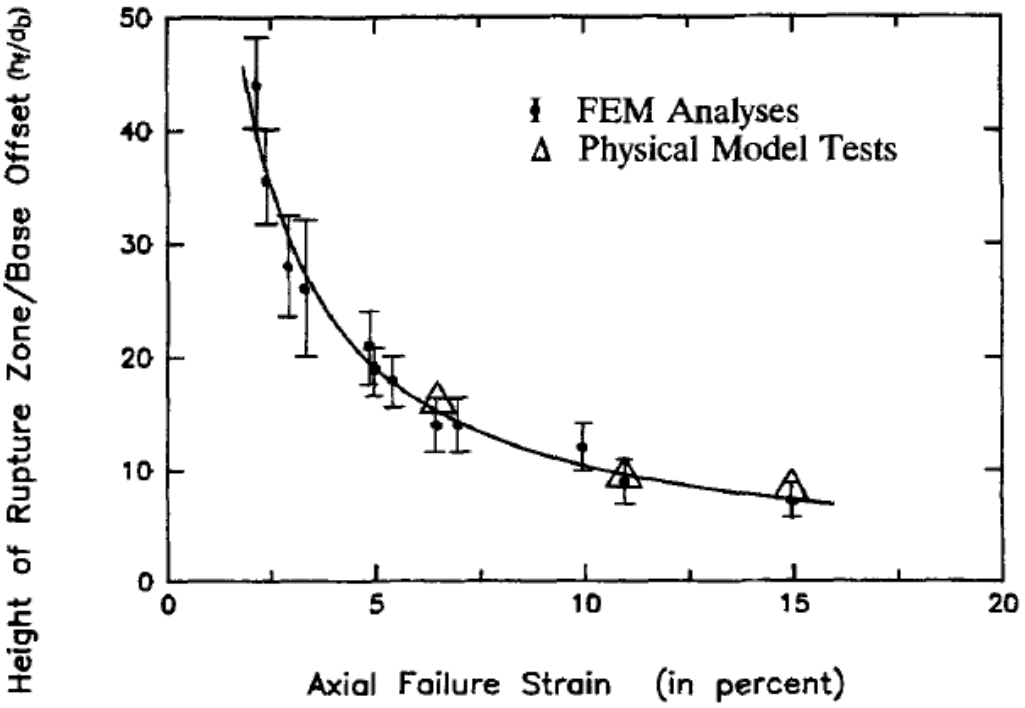

Figure D-8-19. Estimated Normalized Height of Shear Rupture Zone as a Function of Clay's Axial Failure Strain (Bray et al. 2004)

An active fault may pass through the reservoir. Fault offset within the reservoir could create a seiche wave capable of overtopping and eroding the dam. Again, it is necessary to develop an event tree, establish return periods for various levels of fault offset, assess the potential for an overtopping wave to develop, and evaluate the likelihood of short duration overtopping to lead to an erosional breach. An initial estimate of wave height equal to the vertical fault offset is probably reasonably conservative in most cases. The reader is referred to Wilson (1972) and Hammack (1973) for additional discussion on modeling seiche waves. However, overtopping failure of a dam due to seiche waves is a relatively improbable failure mode which is only considered when seismotectonic specialists indicate a high likelihood for development of a seiche wave.

D-8.15 Accounting for Uncertainty

Sensitivity analysis or other appropriate uncertainty analysis methods can be used to explicitly show how uncertainty influences the risk estimate. Reclamation and USACE utilize a suite of scalable assessment approaches that provide information to promote critical thinking and guide a

risk analyst's judgment. For periodic assessment of risks (e.g., Comprehensive Review and Periodic Assessments), simplified event trees are generally developed, and probabilities estimated directly for each branch of the event tree using judgment and subjective probability estimates (see Chapter I-6 Subjective Probability and Expert Elicitation) based on the available information for a particular dam. With a little more effort, uncertainty can be treated to a limited extent with sensitivity analysis by considering likely low, best, and high estimates for key variables. For example, the probability of liquefaction can be estimated as a function of blow count with high, median, and low values, based on the Idriss and Boulanger (2010) liquefaction triggering correlation, for selected load ranges. Crest loss can be estimated based on estimated deformation as a fraction of dam height with high, median, and low values, to determine if the remnant crest is overtopped. A similar process can be made for the probability of failure due to overtopping or internal erosion through cracks (if freeboard remains). A range for annual probability of failure can be calculated using all of the likely low estimates and all of the likely high estimates. Appropriate weighting factors can also be assigned to the low, best, and high estimates to obtain the "best estimate" of annual probability of failure.

The process frequently used for Issue Evaluation (and other higher levels of risk assessment) is typically much more detailed and requires many steps of analysis. Uncertainty is accounted for in the calculations by assigning probability distribution functions for important variables in the risk analysis, such as the representative SPT blow count, the amount of deformation that would occur with a given loading, or the probability of some event, such as the embankment filter being disrupted. Spreadsheet cells or event tree branches are described in terms of a probability distribution rather than a discrete value. Then, a Monte Carlo simulation is performed (typically with 10,000 iterations) to develop a probability distribution for the annual probability of failure and average annual life loss. In some cases, the Monte Carlo model may require calculations and sampling of parameters outside of the event tree. For example, the probability of liquefaction, crest deformation (settlement), and the likelihood of deformation exceeding freeboard all can involve calculations, as opposed to simpler models where the only values with distributions are event probabilities. The more complex procedure may be of great value when the breach probability is very sensitive to small changes in physical quantities, like the reservoir elevation at

the time of the earthquake, the amount of settlement, or the residual undrained shear strength. The steps or general process for higher levels of risk assessment are described below.

D-8.15.1 Step 1

The first step is to gather and assess all available information to generate a belief about liquefaction probability. An understanding of site geology and judgment regarding depositional environment, layering, and material properties leads to selection of a "representative" distribution for SPT blow count. The probability density function used to model SPT blow count can be a compilation of many pieces of information rather than just a statistical representation of a large sample of blow count data. There may be extensive SPT data for some sites, but more often there are limited SPT data or no SPT data at all. BPT, CPT, density or shear wave velocity measurements, and general geologic information all influence judgment used to create the representative blow count distribution. An industry-standard functional relationship between CSR and SPT blow count forms the basis of the liquefaction probability estimate, as depicted in Figure D-8-20.

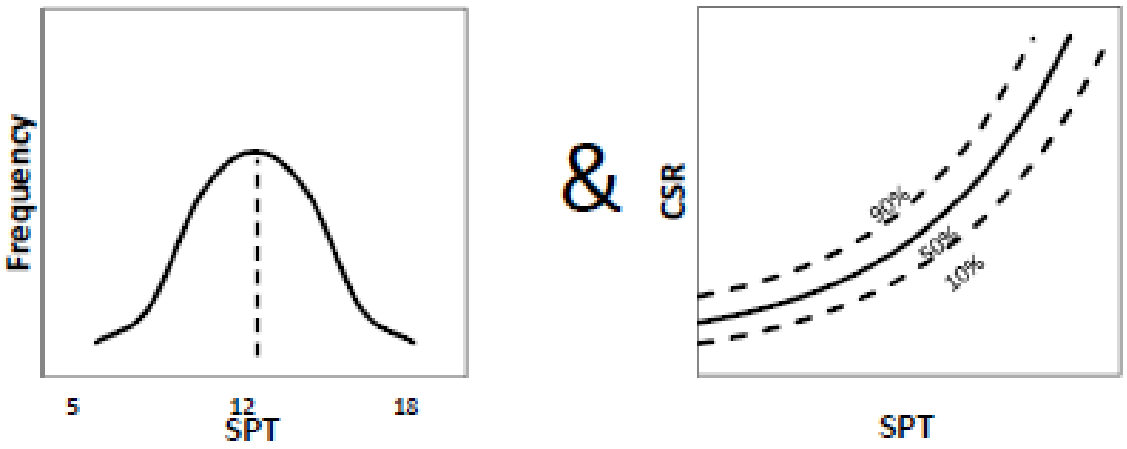

Figure D-8-20. Blow Count Distribution and Liquefaction Probability

D-8.15.2 Step 2

For the second step, a residual shear strength using Seed and Harder (1990) or Idriss and Boulanger (2008), or combination of both relationships, is assigned to the liquefiable materials. The uncertainty in residual shear strength for a given blow count is modeled using a random variable that captures the upper, lower, and best estimate, as depicted in Figure D-8-21.

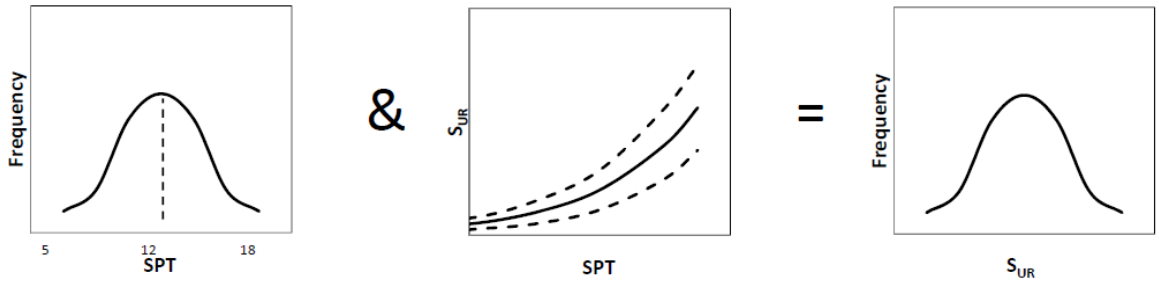

Figure D-8-21. Relationship between Frequency and Residual Shear Strength Relationship

D-8.15.3 Step 3

For each range of ground motion considered, a functional relationship between residual shear strength and crest deformation is constructed from the results of dynamic deformation analysis. An example of a functional relationship for a single discrete range of ground motion is provided in Figure D-8-22. Residual shear strength is varied in a parametric study of seismically-induced deformations to obtain estimates for potential crest deformations. Upstream and downstream slope instabilities are both considered, as is the possibility that the entire embankment could be pushed downstream in a translational shear failure.

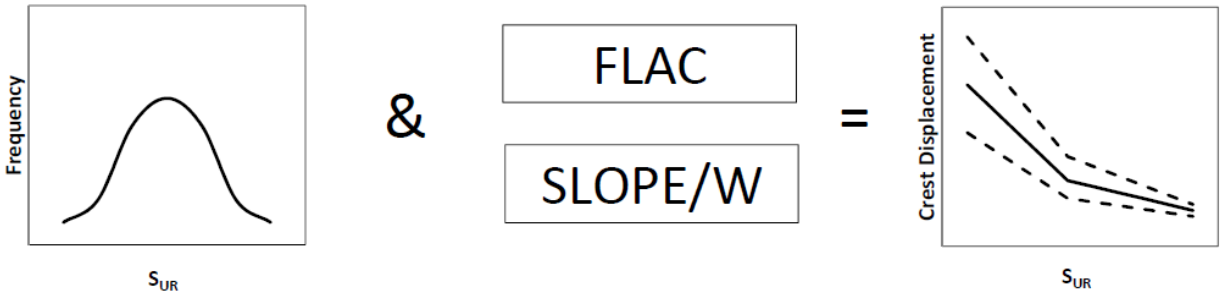

Figure D-8-22. Functional Relationship between Crest Deformation and Residual Shear Strength

D-8.15.4 Step 4

The reservoir elevation could be anywhere in its operating range when an earthquake occurs. Historical reservoir operation data indicates the frequency at which the reservoir has been at a given elevation and is used to create the reservoir operating curve (stage-duration curve), which is used to predict how much freeboard is likely to exist when an earthquake does occur.. Given probability distributions for the pre-earthquake freeboard and the likelihood for crest

deformation, the likelihood for post-earthquake freeboard is calculated as a joint probability of the two, as depicted in Figure 27-23.

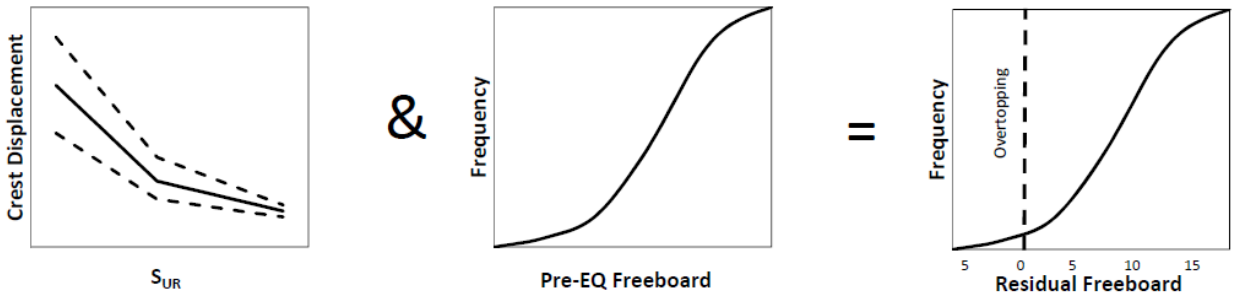

Figure D-8-23. Calculation of Residual Freeboard

D-8.15.5 Step 5

Given post-earthquake freeboard, the likelihood for continuing breach development by overtopping and down-cutting erosion is assessed using another intuitive functional relationship, as depicted in Figure 27-24. The reasoning used to form the shape of this relationship is as follows:

- If crest deformation is greater than initial freeboard, overtopping and erosion is virtually certain. Failure from this point would most likely take place rapidly, depending on the degree of overtopping and the erodibility of the embankment materials.
- If crest deformation is only slightly less than initial freeboard, there may be interconnected cracks in the crest, open and deep enough to intersect the reservoir. Water flowing in these cracks would have to flow fast enough and with sufficient quantity to be capable of eroding and transporting embankment material. Upstream shell or crack-stopping materials would have to fail to perform a self-healing, filter-forming operation, and a functional downstream filter zone would have to be missing in the original design or displaced/disrupted by crest deformation. Whether breach formation would continue would depend on the depth and velocity of water in the open cracks. Also, there is a possibility that human interventions might be successful.

The actual freeboard amount responsible for the various breach-continuation likelihoods would also depend on the amount of crest deformation. Post-earthquake freeboard values transpiring from different amounts of pre-earthquake freeboard pose different potential for erosional failure.

If crest deformation is much less than initial freeboard, the dam crest is not likely to be in jeopardy, but internal erosion failure modes at other locations within the dam or foundation could become an issue, particularly for embankments already considered to be in marginally poor condition.

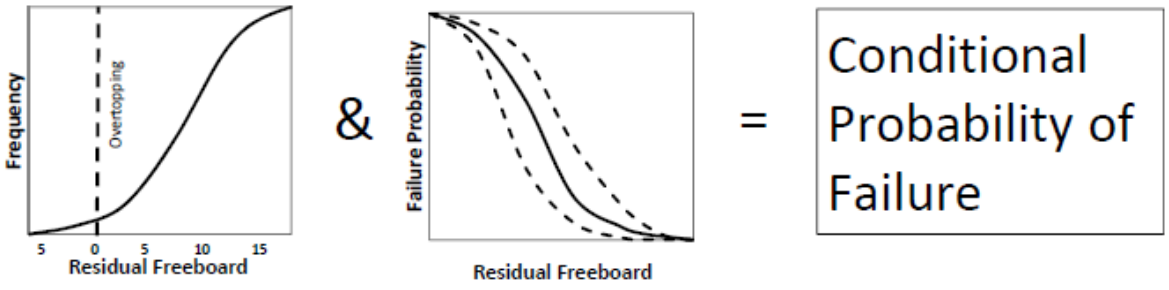

Figure D-8-24. Calculation for Probability of Failure

The curve representing failure likelihood as a function of post-earthquake residual freeboard may include some probability of failure with positive freeboard remaining. This represents the likelihood of rapid erosion through a severely damaged crest, rather than slower seepage erosion through earthquake-induced cracks, which was covered earlier in this section.

D-8.16 Exercise

Using the event tree in Figure D-8-6 as a guide, develop an event tree to assess the risk probability of failure for the failure mode of deformation leading to transverse cracking and internal erosion through the cracks.

D-8.17 References

Bray, J. D., and Sancio, R. B. (2006). "Assessment of the liquefaction susceptibility of fine-grained soils," *Journal of Geotechnical and Geoenvironmental Engineering*, American Society of Civil Engineers, 132(9), 1165–1177.

Bray, J. D., R.B. Seed, and Seed, H. B. (2004). “Analysis of earthquake fault rupture propagation through cohesive soil,” *Journal of Geotechnical and Geoenvironmental Engineering*, American Society of Civil Engineers, 120(3), 562-580.

Bray, J. D., and Travasarou, T. (2007). “A simplified procedure for estimating earthquake-induced deviatoric slope displacements,” *Journal of Geotechnical and Geoenvironmental Engineering*, American Society of Civil Engineers, 133(4), 381-392.

Boulanger, R. W. and Idriss, I. M. (2014). *CPT and SPT Based Liquefaction Triggering Procedures*, Report No. UCD/CGM-14/01, Department of Civil and Environmental Engineering, University of California at Davis, Davis, CA.

Boulanger, R. W. and Idriss, I. M. (2004). *Evaluating the Potential for Liquefaction or Cyclic Failure of Silts and Clays*, Report No. UCD/CGM-04/01, Department of Civil and Environmental Engineering, University of California at Davis, Davis, CA.

Bureau of Reclamation (2005). “Estimating risk from seismic loading of embankment dams and foundations,” *Risk Analysis Methodology*, Appendix J, Technical Service Center, Denver, CO.

Cetin, K. O., Seed, R. B., Moss, R. E. S., Der Kiureghian, A. K., Tokimatsu, K., Harder, L. F., and Kayen, R. E. (2000). *Field Performance Case Histories for SPT-Based Evaluation of Soil Liquefaction Triggering Hazard*, Report No. UCB/GT-2000/09, University of California at Berkeley, Berkeley, CA.

Cetin, K. O., Seed, R. B., Der Kiureghian, A., Tokimatsu, K., Harder, L. F., Kayen, R. E., and Moss, R. E. S. (2004). “Standard penetration test-based probabilistic and deterministic assessment of seismic soil liquefaction potential, *Journal of Geotechnical and Geoenvironmental Engineering*, American Society of Civil Engineers, 130(12), 1314-1340.

Davis, C. A. (1997). *Response of the San Fernando power plant tailrace to the 1994 Northridge earthquake and recommended repairs*, Publication No. AX 215-48, DSR#68514, City of Los Angeles, Department of Water and Power, Water Supply Division, Los Angeles, CA.

Fell, R., Foster, M., Cyganiewicz, J., Sills, G., Vroman, N., and Davidson, R. (2008). *Risk Analysis for Dam Safety: A Unified Method for Estimating Probabilities of Failure of Embankment Dams by Internal Erosion and Piping*, URS Australia Pty. Ltd., Sydney, New South Wales, Australia.

FMSM Engineers (2007). A Simplified Tool for Assessing the Deformation of Embankment Dams and Levees on Liquefied Soils, Final Report, prepared by FMSM Engineers for the U. S. Army Corps of Engineers, Louisville, Kentucky.

Forster, I. R., and MacDonald, R. B. (1998). "Post-earthquake response procedures for embankment dams: Lessons from the Loma Prieta earthquake," *ANCOLD Bulletin No. 109,* Australian National Committee on Large Dams, 46-64.

Gillette, D. R. (2010). "On the use of empirical correlations for estimating the residual undrained shear strength of liquefied soils in dam foundations," *Proc., Fifth International Conference on Recent Advances in Geotechnical Earthquake Engineering and Soil Dynamics*, San Diego, California.

Hammack, J. L. (1973). "A note on tsunamis: Their generation and propagation in an ocean of uniform depth," *Journal of Fluid Mechanics*, Cambridge University Press, 60(4), 769-799.

Harder, L. F. Jr. (1991). "Performance of earth dams during the Loma Prieta earthquake," *Proc., Second International Conference on Recent Advances in Geotechnical Earthquake Engineering and Soil Dynamics*, Saint Louis, Missouri.

Idriss, I. M. and Boulanger R. W. (2010). *SPT-based Liquefaction Triggering Procedures*, Report No. UCD/CGM-10/02, University of California at Davis, Davis, CA.

Idriss, I. M. and Boulanger, I. M. (2008). *Soil Liquefaction during Earthquakes*. MNO-12, Earthquake Engineering Research Institute, Oakland, CA.

Liao, S. S. C., Veneziano, D., and Whitman, R. V. (1988). "Regression models for evaluating liquefaction probability," *Journal of Geotechnical Engineering*, American Society of Civil Engineers, 114(4), 389-409.

Makdisi, F. I., and Seed, H. B. (1978). "Simplified procedure for estimating dam and embankment earthquake-induced deformations," *Journal of Geotechnical Engineering Division*, American Society of Civil Engineers, 104(7), 849-867.

Newmark, N.M., (1965). "Effects of earthquakes on dams and embankments," Géotechnique, 15(2), 139-160.

Olson, S. M. and Stark, T. D. (2002). "Liquefied strength ratio from liquefaction case histories," *Canadian Geotechnical Journal*, National Research Council Canada, 39(3), 629–647.

Olson, S. M. and Stark, T. D. (2003). "Yield strength ratio and liquefaction analysis of slopes and embankments," Journal *of Geotechnical and Geoenvironmental Engineering*, American Society of Civil Engineers, 129(8), 727–737.

Pells, S. and Fell, R. (2003). "Damage and cracking of embankment dams by earthquake and the implications for internal erosion and piping." *Proc., 21st Internal Congress on Large Dams*, Montreal. ICOLD, Paris Q83-R17, International Commission on Large Dams, Paris.

Seed, R. B., Cetin, K. O., Moss, R. E. S., Kammerer, A. M., Wu, J., Pestana, J. M., Riemer, M. F., Sancio, R. B., Bray, J. D., Kayen, R. E., and Faris, A. (2003). "Recent advances in soil liquefaction engineering: A unified and consistent framework," *Proc., 26th Annual ASCE Los Angeles Geotechnical Spring Seminar*, Long Beach, CA.

Seed, R. B., and Harder, L. F. (1990). "SPT-based analysis of cyclic pore pressure generation and undrained residual strength," *H. B. Seed Memorial Symposium*, Berkeley, CA, BiTech Publishing, Ltd., Vol. 2, 351-376.

Seed, H. B., Lee, K. L., Idriss, I. M., and Makdisi, F. I. (1975). "The slides in the San Fernando Dams during the earthquake of February 9, 1971," *Journal of the Geotechnical Engineering Division*, American Society of Engineers, 101(7), 651-688.

Seed, H. B., Lee, K. K., and Idriss, I. M. (1969). "Analysis of Sheffield Dam failure," *Journal of the Soil Mechanics and Foundations Division*, American Society of Civil Engineers, 95(6), 1453-1490.

Swaisgood, J. R. (2014). "Behavior of embankment dams during earthquake," *Journal of Dam Safety*, ASDSO, 12(2): 35-44.

Swaisgood, J. R. (2003). "Embankment dam deformations caused by earthquakes," *Proc., 2003 Pacific Conference on Earthquake Eng.*, Christchurch, New Zealand.

Swaisgood, J. R. (1998). "Seismically-induced deformation of embankment dams," *Proc., 1998 U.S. National Conference on Earthquake Engineering*, Seattle, Washington.

Watson-Lamprey, J., and Abrahamson, N. (2006). "Selection of ground motion time series and limits on scaling," *Soil Dynamics and Earthquake Engineering*. 26(2006), 477–482.

Wilson, B. W. (1972). "Seiches," *Advances in Hydroscience*, Chow, U.T. (editor), Academic Press, New York, New York, Vol. 8.

Youd, T. L., Hansen, C. M., and Bartlett, S. F. (2002). "Revised multilinear regression equations for prediction of lateral spread displacement," *Journal of Geotechnical and Geoenvironmental Engineering*, American Society of Civil Engineers, 128(12), 1007-1017.